

12-1-2023

## ABCB5+ mesenchymal stromal cells therapy protects from hypoxia by restoring Ca<sup>2+</sup> homeostasis in vitro and in vivo

Kaixuan Yan

Jiaying Zheng

Mark Andreas Kluth

Lin Li

Christoph Ganss

*See next page for additional authors*

Follow this and additional works at: <https://ro.ecu.edu.au/ecuworks2022-2026>



Part of the [Therapeutics Commons](#)

---

[10.1186/s13287-022-03228-w](https://doi.org/10.1186/s13287-022-03228-w)

Yan, K., Zheng, J., Kluth, M. A., Li, L., Ganss, C., Yard, B., ... & Keese, M. (2023). ABCB5+ mesenchymal stromal cells therapy protects from hypoxia by restoring Ca<sup>2+</sup> homeostasis in vitro and in vivo. *Stem Cell Research & Therapy*, 14, Article 24.

<https://doi.org/10.1186/s13287-022-03228-w>

This Journal Article is posted at Research Online.

<https://ro.ecu.edu.au/ecuworks2022-2026/2003>

---

**Authors**

Kaixuan Yan, Jiaxing Zheng, Mark Andreas Kluth, Lin Li, Christoph Ganss, Benito Yard, Richard Magdeburg, Markus H. Frank, Prama Pallavi, and Michael Keese

RESEARCH

Open Access



# ABCB5<sup>+</sup> mesenchymal stromal cells therapy protects from hypoxia by restoring Ca<sup>2+</sup> homeostasis in vitro and in vivo

Kaixuan Yan<sup>1,2</sup>, Jiaying Zheng<sup>1,2</sup>, Mark Andreas Kluth<sup>3</sup>, Lin Li<sup>1,2</sup>, Christoph Ganss<sup>3,4</sup>, Benito Yard<sup>5</sup>, Richard Magdeburg<sup>11</sup>, Markus H. Frank<sup>7,8,9,10</sup>, Prama Pallavi<sup>1,2,11\*†</sup>  and Michael Keese<sup>1,2,6,11\*†</sup>

## Abstract

**Background** Hypoxia in ischemic disease impairs Ca<sup>2+</sup> homeostasis and may promote angiogenesis. The therapeutic efficacy of mesenchymal stromal cells (MSCs) in peripheral arterial occlusive disease is well established, yet its influence on cellular Ca<sup>2+</sup> homeostasis remains to be elucidated. We addressed the influence of ATP-binding cassette subfamily B member 5 positive mesenchymal stromal cells (ABCB5<sup>+</sup> MSCs) on Ca<sup>2+</sup> homeostasis in hypoxic human umbilical vein endothelial cells (HUVECs) in vitro and in vivo.

**Methods** Hypoxia was induced in HUVECs by Cobalt (II) chloride (CoCl<sub>2</sub>) or Deferoxamine (DFO). Dynamic changes in the cytosolic- and endoplasmic reticulum (ER) Ca<sup>2+</sup> and changes in reactive oxygen species were assessed by appropriate fluorescence-based sensors. Metabolic activity, cell migration, and tube formation were assessed by standard assays. Acute-on-chronic ischemia in Apolipoprotein E knock-out (ApoE<sup>-/-</sup>) mice was performed by double ligation of the right femoral artery (DFLA). ABCB5<sup>+</sup> MSC cells were injected into the ischemic limb. Functional recovery after DFLA and histology of gastrocnemius and aorta were assessed.

**Results** Hypoxia-induced impairment of cytosolic and ER Ca<sup>2+</sup> were restored by ABCB5<sup>+</sup> MSCs or their conditioned medium. Similar was found for changes in intracellular ROS production, metabolic activity, migratory ability and tube formation. The restoration was paralleled by an increased expression of the Ca<sup>2+</sup> transporter Sarco-/endoplasmic reticulum ATPase 2a (SERCA2a) and the phosphorylation of Phospholamban (PLN). In acute-on-chronic ischemia, ABCB5<sup>+</sup> MSCs treated mice showed a higher microvascular density, increased SERCA2a expression and PLN phosphorylation relative to untreated controls.

**Conclusions** ABCB5<sup>+</sup> MSCs therapy can restore cellular Ca<sup>2+</sup> homeostasis, which may beneficially affect the angiogenic function of endothelial cells under hypoxia in vitro and in vivo.

**Keywords** Peripheral artery disease, Mesenchymal stromal cells, Stem cell therapy, Hypoxia, Calcium ion, Endothelial cells, Angiogenesis

<sup>†</sup>Prama Pallavi and Michael Keese have contributed equally

\*Correspondence:

Prama Pallavi

prama.pallavi@medma.uni-heidelberg.de

Michael Keese

Michael.keese@umm.de

Full list of author information is available at the end of the article



## Background

Peripheral artery disease (PAD) is characterized by decreasing in the supplying blood to the upper or lower limbs because of the narrowing or blockage of the arteries [1]. Our research focuses on the PAD that affects the leg(s). Hypoxia in the muscle and soft tissue of the leg(s) due to poor perfusion is one of the main characteristics of the pathogenesis of PAD [2]. Exposure to hypoxia activates the angiogenic function of endothelial cells (ECs) [3–5]. This process plays a pivotal role in the pathophysiology of various diseases such as cerebral ischemia, myocardial infarction, and PAD [6, 7]. However, the natural course and the relatively poor prognosis of PAD indicate the lower capillary density induced by hypoxia [8, 9].

Over the past two decades, stem cells have emerged as an alternative for the treatment of patients with PAD. Reduction in resting pain, pain-free walking time and ulcer healing were reported after autologous stem cells treatment of critical limb ischemia in the patients [10–12]. However, autologous stem cells treatment is still facing some challenges that hamper its implementation as a mainstay of treatment. Because the majority of the PAD patients are elderly and often present other co-morbidities, harvesting autologous stem cells from such patients is tedious as the amount and potency of stem cells is generally reduced in elderly donors. It should also be underscored that autologous stem cells treatment in PAD patients did not reduce rates of limb amputation [13, 14]. These shortcomings of autologous stem cells, therefore, warrant further studies on the efficacy of other types of stem cells.

The MSCs were normally isolated from the bone marrow or adipose tissue of people of different ages and morbidities which may lead to the inhomogeneity of functional properties of MSCs while the ATP-binding cassette subfamily B member 5 positive mesenchymal stromal cells (ABCB5<sup>+</sup> MSCs) were manufactured by TICEBA GmbH from strict health skin tissue donations of donors whose age  $\leq 50$  years old, which could guarantee reliable and reproducible cell quality and functionality [15]. ABCB5<sup>+</sup> MSCs express mesenchymal lineage markers (CD90, CD105 and CD73) [16], lack hematopoietic lineage markers CD34, CD14, CD20 and CD45; and show significantly increased adipogenic, osteogenic and chondrogenic differentiation potential [16]. In addition to this, ABCB5<sup>+</sup> MSCs exhibit immunomodulatory effects through interaction with macrophages [17] and regulatory T lymphocytes [18]. They exhibit a strong paracrine capacity including interleukin 1 receptor antagonist [16, 17] and under hypoxia ABCB5<sup>+</sup> MSCs secrete vascular endothelial growth factor (VEGF) and can trans-differentiate into CD31<sup>+</sup> ECs [16]. ABCB5<sup>+</sup> MSCs suppress reactive oxygen species (ROS) release and extracellular trap

formation from activated human peripheral neutrophils [19]. Thus, the immunomodulatory, paracrine as well as trans-differentiation capabilities of ABCB5<sup>+</sup> MSCs make them an ideal stem cell therapy candidate to restore the tissue integrity after hypoxic injury in PAD.

Under physiological conditions, hypoxia or low oxygen tension favors the stabilization of hypoxia inducing factor (HIF)-1 $\alpha$  that together with HIF-1 $\beta$  forms the active HIF-1 complex, required for the expression of a number of pro-angiogenic genes [3–5, 20, 21]. In PAD patients, however, this neovascular response seems to be insufficient for adequately reperfusion the ischemic tissue. Apart from angiogenesis, chronic hypoxia also adversely affects the mitochondrial-endoplasmic reticulum (ER) crosstalk by changing ROS and Ca<sup>2+</sup> homeostasis [22–28], thereby favoring cell dysfunction, apoptosis and end organ-damage [6, 29].

Ca<sup>2+</sup> homeostasis is essential to regulate a wide variety of cellular processes including angiogenesis [34]. It involves a tight regulation of uptake and release of Ca<sup>2+</sup> into and from intracellular organelles such as the ER as well as a controlled influx from the extracellular environment [30, 31]. Arnould et al. and Suresh et al. both found that hypoxia could induce the extracellular Ca<sup>2+</sup> influx that leads to an increase in cytosolic (Cyto) Ca<sup>2+</sup> concentration [22, 23]. The hypoxia could liberate Ca<sup>2+</sup> from ER by the generation of mitochondrial ROS [23, 32]. Paul T and his colleagues found that the ER Ca<sup>2+</sup> release was needed during the process of angiogenesis [24]. However, the Cyto Ca<sup>2+</sup> overloading induced by hypoxia could lead to angiogenic dysfunction and apoptosis [26–28]. The damaging effect of hypoxia on ER Ca<sup>2+</sup> homeostasis in ECs during angiogenesis and the influence of ABCB5<sup>+</sup> MSCs on Ca<sup>2+</sup> homeostasis in hypoxic ECs have not been extensively studied. In the present study, we test the hypothesis that ABCB5<sup>+</sup> MSCs yield a beneficial effect on angiogenesis by restoring Ca<sup>2+</sup> homeostasis in the ECs. We tested this hypothesis by addressing if ABCB5<sup>+</sup> MSCs alleviate the overloading of Cyto Ca<sup>2+</sup> and restore ER Ca<sup>2+</sup> in hypoxic HUVECs. We further evaluated the effect of ABCB5<sup>+</sup> MSCs on hypoxia-induced ROS burden in HUVECs. Finally, we tested if ABCB5<sup>+</sup> MSCs restore ER Ca<sup>2+</sup> using the Sarco-/endoplasmic reticulum ATPase 2a (SERCA2a)- Phospholamban (PLN) axis in both in-vitro cell models as well as in-vivo hind limb ischemia model in Apolipoprotein E knock-out (ApoE<sup>-/-</sup>) mice, which model chronic on acute hypoxia.

## Materials and methods

### Cell lines and cell culture

Human umbilical cord vein endothelial cells (HUVECs) used in this project were isolated from human umbilical cords which were kindly provided by the Department of

Obstetrics and Gynecology, University Medical Center Mannheim, University of Heidelberg, Mannheim, Germany. The isolation procedure was approved by the local ethics committee (Ethikkommission II der Medizinische Fakultät Mannheim AZ 2015-518N-MA). The HUVECs isolation was performed as previously described [33]. The identity of the isolated cells was confirmed by immunofluorescence staining for classical endothelial markers-CD31, von Willebrand factor (vWF) and VE-Cadherin. The HUVECs were cultured on 1% gelatin-coated (Sigma-Aldrich, Germany, 9000-70-8) culture flasks in endothelial cell growth medium (Provitro, Germany, 2011101) supplemented with 5% fetal bovine serum (FBS, Gibco, Brazil, 10270106) and 1% penicillin and streptomycin (P/S, Sigma-Aldrich, Germany, 2011101).

ABCB5<sup>+</sup> MSCs were manufactured by TICEBA GmbH (Heidelberg, Germany) as described before [15]. ABCB5<sup>+</sup> MSCs were cultured in Ham's F-10 Medium (Biochrom GmbH, Germany, F0715) with 10% of FBS, 1% of P/S and 2 mM L-glutamine (Roth, Germany, 56-85-9).

ABCB5<sup>+</sup> MSCs and HUVECs were all incubated at 37 °C in a humidified incubator with 5% CO<sub>2</sub>. The medium was changed every two days. HUVECs between passages 2–5 and the ABCB5<sup>+</sup> MSCs between passages 1–3 were used for all experiments [15].

#### **In-vitro hypoxia and co-culture**

In-vitro hypoxia was modeled by treating HUVECs with 80 μM Cobalt (II) chloride (CoCl<sub>2</sub>, Sigma-Aldrich, Germany, C8661, Additional file 1: Fig. S1A–D) or 120 μM Deferoxamine (DFO, Sigma-Aldrich, Germany, D9533, Additional file 2: Fig. S2A–D) for 4 h. In another experimental condition to irreversibly inhibit SERCA2a, HUVECs were treated with 3 μM Thapsigargin (TG, Sigma-Aldrich, Germany, T9033, Additional file 3: Fig. S3A) for 4 h.

In this research, two kinds of therapeutic approaches for the application of ABCB5<sup>+</sup> MSCs as previously reported [34, 35]. The first approach is to coculture the HUVECs coculture with ABCB5<sup>+</sup> MSCs in the coculture system (ABCB5<sup>+</sup> MSC-CO). The second approach is to use the ABCB5<sup>+</sup> MSCs- conditioned medium to treat the HUVECs (ABCB5<sup>+</sup> MSC-CM). For the ABCB5<sup>+</sup> MSC-CO system, 0.5 × 10<sup>4</sup> ABCB5<sup>+</sup> MSCs per cm<sup>2</sup> were seeded in cell culture inserts fit for 6-well (4.5 cm<sup>2</sup>/insert, Greiner Bio-One, Germany, 657640) and 24-well plates (0.3 cm<sup>2</sup>/insert, Greiner Bio-One, Germany, 657640). 2 × 10<sup>4</sup> HUVECs per cm<sup>2</sup> were seeded in gelatin-coated 6-well and 24-well plates (9.6 cm<sup>2</sup>/well and 1.9 cm<sup>2</sup>/well) as previously reported [36–38]. The co-culture was performed in a 1:1 mix of HUVECs and ABCB5<sup>+</sup> MSCs medium. ABCB5<sup>+</sup> MSC-CM was collected as previously reported [35]. The conditioned medium was aliquoted

and stored at –80 °C for later use. In all the in-vitro cell culture experiments HUVECs were first treated with either CoCl<sub>2</sub> or DFO or TG for 4 h and afterward cocultured with ABCB5<sup>+</sup> MSCs or cultured in ABCB5<sup>+</sup> MSC conditioned medium with the continued presence of CoCl<sub>2</sub> or DFO or TG.

#### **MTT assay**

MTT (3-(4, 5-dimethyl thiazolyl-2)-2, 5-diphenyltetrazolium bromide, Sigma, USA, M2128) assays were performed to detect the metabolic activity of HUVECs. Briefly, log-phase HUVECs were seeded into a gelatin-coated 24-well plate (1 × 10<sup>6</sup> cells/well). 24 h post-seeding cells were first treated with either 80 μM CoCl<sub>2</sub> or 120 μM DFO or 3 μM TG for 4 h. Thereafter, HUVECs were either cultured in ABCB5<sup>+</sup> MSC-CM or cocultured with ABCB5<sup>+</sup> MSCs in presence of 80 μM CoCl<sub>2</sub>, 120 μM DFO or 3 μM TG for another 24 h. Afterward, 20 μL of the MTT dye (0.5 mg/mL) was added to each well and cells were incubated further for a period of 4 h. The formazan salts were dissolved with 100 μL freshly prepared MTT solvent constituting 40% of Dimethyl sulfoxide (DMSO, Roth, Germany, HN47.1), 40% of 10%-sodium dodecyl sulfate (SDS, Roth, Germany, 0183.3), 20% of DPBS, and 1.2% of Acetic acid (Roth, Germany, 6755.1) and absorbance (wavelength 540 nm, reference length 630 nm) was recorded with a Tecan multimode microplate reader (Spark, Switzerland).

#### **Scratch assay**

Scratch assays were performed to evaluate the cell migration property of HUVECs. To this end, 1 × 10<sup>6</sup> HUVECs per well were seeded into the 1% Gelatin-coated 24-well plate to establish a single cell monolayer in medium supplemented with 3% FBS. After overnight incubation, the cells were first treated with either 80 μM CoCl<sub>2</sub> or 120 μM DFO or 3 μM TG for 4 h. For CoCl<sub>2</sub>, DFO and TG treated cells monolayer was scratched along a straight line by using a 200 μL pipette tip. For the ABCB5<sup>+</sup> MSC groups, HUVECs were either cocultured with the ABCB5<sup>+</sup> cells or cultured in ABCB5<sup>+</sup> CM after the 4 h treatments with CoCl<sub>2</sub> or DFO or TG. The HUVECs treatment with CoCl<sub>2</sub> or DFO or TG during ABCB5<sup>+</sup> MSC therapy was continued. The photos of the monolayer were taken at 0 h, 6 h, 12 h, and 24 h by an inverted microscope (Axiovert 200 M; Zeiss, Jena, Germany). The gap area was quantitatively evaluated using ImageJ software (version 1.52, Bethesda, USA).

#### **Tube formation assay**

The HUVECs tube formation assay was employed as reported previously [39]. Briefly, HUVECs were first

treated with 80  $\mu\text{M}$   $\text{CoCl}_2$ , 120  $\mu\text{M}$  DFO or 3  $\mu\text{M}$  TG for 4 h. Subsequently, cells were harvested and diluted to  $2.5 \times 10^4$  cells/mL in medium supplemented with 1% FBS and seeded into the matrigel basement membrane matrix phenol red-free (Corning, USA, 356,237) pre-coated 24-well plates ( $1 \times 10^5$  cells/well). Afterward, HUVECs were either co-cultured with ABCB5<sup>+</sup> MSCs or cultured in ABCB5<sup>+</sup> MSC-CM, and treated with 80  $\mu\text{M}$   $\text{CoCl}_2$ , 120  $\mu\text{M}$  DFO or 3  $\mu\text{M}$  TG was continued for 24 h. Images were taken by an inverted microscope after 6 h incubation. The number of HUVECs meshes and junctions were analyzed by the angiogenesis analyzer plugin for ImageJ.

### Cloning, virus production and transduction

#### D1ER

D1ER, genetically encoded fluorescence resonance energy transfer (FRET) based ER  $\text{Ca}^{2+}$  biosensor which contains enhanced yellow fluorescent protein (YFP: Ex 514 nm/Em 527 nm) and enhanced cyan fluorescent protein (CFP: Ex 430 nm/Em 474 nm) [40] was used to study changes in ER  $\text{Ca}^{2+}$  [40]. It was synthesized by Genewiz from Merck Sigma Aldrich in pUC57 with BamHI and XbaI restriction sites and further cloned into pHR'SIN-cPPT-SEW via BamHI and XbaI restriction sites. Lentivirus particles were produced as previously described [41, 42] and HUVECs were transduced. The ratio of FRET was calculated by dividing CFP-intensity by YFP-intensity both detected from D1ER (FRET ratio = YFP/CFP). This ratio represented the dynamic changes in ER  $\text{Ca}^{2+}$  concentration [43].

#### roGFP3

It was used to monitor the dynamic changes of ROS signaling [44]. Lentivirus encoding roGFP3 were generated and HUVECs were transduced as previously described [41].

The stable expression of D1ER and roGFP3 in HUVECs was verified over passages by qualitative assessment of fluorescence intensity. Up to three passages after transduction, no evident expression changes were observed.

#### Measurement of ER $\text{Ca}^{2+}$

HUVECs transduced with the D1ER sensor were seeded into the 1% gelatin-coated 24-well-plates ( $3.8 \times 10^4$  cells per well). 24 h post seeding cells were treated with 80  $\mu\text{M}$   $\text{CoCl}_2$ , 120  $\mu\text{M}$  DFO and 3  $\mu\text{M}$  TG for 4 h. Thereafter, cells were either co-cultured with ABCB5<sup>+</sup> MSCs or cultured in ABCB5<sup>+</sup> MSC-CM for 24 h. The fluorescence intensity of CFP and YFP were detected by a Tecan multimode microplate reader every 2 h. In addition to live cell measurements, ER  $\text{Ca}^{2+}$  was also measured by confocal microscopy. To this end HUVECs transduced with D1ER

sensor were seeded into the 1% gelatin-coated 15 mm coverslips in 24-well-plates ( $3.8 \times 10^4$  cells per well) and the experiment was set up as described above. After the 24 h treatment, cells were fixed with 4% paraformaldehyde (PFA) and imaged by an SP5 microscope system (Leica, Germany) to detect the fluorescence emitted by YFP and CFP. The images were analyzed by NIH ImageJ version 1.52 software to compare the FRET ratio among the different groups.

#### Measurement of Cyto $\text{Ca}^{2+}$

Fura-2-acetoxymethyl ester (Fura 2-AM, Biotium, USA, 50,033) was used to detect changes in the Cyto  $\text{Ca}^{2+}$  as previously described [18]. These experiments were performed in two formats.

In the first experiment,  $3.8 \times 10^4$  HUVECs seeded per well in 24-well plates were treated with 80  $\mu\text{M}$   $\text{CoCl}_2$  or 120  $\mu\text{M}$  DFO or 3  $\mu\text{M}$  TG or 100  $\mu\text{M}$  hydrogen peroxide ( $\text{H}_2\text{O}_2$ ) in HHBSS without  $\text{Ca}^{2+}$  for first 2 h. Afterward buffer was changed to HHBSS with  $\text{Ca}^{2+}$  for the following 2 h. 100  $\mu\text{M}$  Ionomycin (Ion, Sigma, Germany, I9657) was also used as the positive control.

In the second experimental setup, cells were treated by 80  $\mu\text{M}$   $\text{CoCl}_2$ , 120  $\mu\text{M}$  DFO, and 3  $\mu\text{M}$  TG for 4 h. After that, they were either co-cultured with ABCB5<sup>+</sup> MSCs or cultured in ABCB5<sup>+</sup> MSC-CM for 24 h, under treatment with 80  $\mu\text{M}$   $\text{CoCl}_2$ , 120  $\mu\text{M}$  DFO or 3  $\mu\text{M}$  TG for 24 h, separately. 100  $\mu\text{M}$  Ion and 100  $\mu\text{M}$   $\text{H}_2\text{O}_2$  served as the positive control. The dynamic changes of Cyto  $\text{Ca}^{2+}$  were detected by monitoring the fluorescence (Em 535 nm) from Fura 2-AM excited by wavelengths of 340 nm and 380 nm on the multimode microplate reader. The fluorescence intensity of Fura 2-AM was monitored by a Tecan multimode microplate reader every 2 h.

#### Measurement of ROS signal

HUVECs expressing roGFP3 were seeded into 24-well-plates ( $1 \times 10^6$  cells/well). One day post seeding cells were first treated with either 80  $\mu\text{M}$   $\text{CoCl}_2$  or 120  $\mu\text{M}$  DFO for 4 h. Afterward, HUVECs were either co-cultured with ABCB5<sup>+</sup> MSCs or cultured in ABCB5<sup>+</sup> MSC-CM for 24 h, and treatment with 80  $\mu\text{M}$   $\text{CoCl}_2$ , 120  $\mu\text{M}$  DFO or 3  $\mu\text{M}$  TG was continued for 24 h. HUVECs treated with 100  $\mu\text{M}$   $\text{H}_2\text{O}_2$  served as the positive control. The dynamic changes in the ratio of fluorescence intensity emitted by roGFP3 were monitored on the Tecan multimode microplate reader as previously described [41].

#### PAD ApoE<sup>-/-</sup> mouse model

All experimental procedures on animals were performed according to the EC guideline EC 2010/63/EU and have been approved by the local German government authority (35-9185.81/G[1]239/18).

8-week-old male ApoE<sup>-/-</sup> mice with the C57BL/6J background were purchased from Charles River Laboratories. The animals were housed in a 12 h light/dark cycle and fed a Western Diet (5% cholesterol and 21% fat) for 12 weeks with free access to food and water.

Mice were anesthetized with a subcutaneous injection (S.C.) of a mixture of Midazolam (5 mg/kg, Ratiopharm, Germany, 44856.01.00), Medetomidine (0.05 mg/mL/kg, Cayman Chemical, USA, 128366-50-7) and fentanyl (0.5 mg/kg, Cayman Chemical, Germany, 437-38-7) before all surgical procedures. Double ligation of the right femoral artery (DLFA) was performed using Ethicon 7-0 sutures (PROLENE, Germany, 8776H) as described previously to simulate an acute-on-chronic model of PAD [45]. Immediately after DLFA, 100  $\mu$ L ABCB5<sup>+</sup> MSCs ( $1 \times 10^8$  cells/mL) suspension was injected into 5 different muscle localizations of the right hind limb (20  $\mu$ L each localization) in the treatment group ( $n = 12$ ). Animals in the control group ( $n = 12$ ) received 100  $\mu$ L normal saline in the same way. For the postoperative analgesia, butorphanol (1 mg/kg, S.C., Q8h, Dolorex, Germany, 42408-82-2) was given to the mice 24 h after DLFA. Drinking water was supplemented with metamizole (24 mg/5 mL of water, corresponding to a dose of 200 mg/kg 4 times daily) to maintain the analgesic effect for 2 days following the DLFA procedure. On the 1st day after the operation, magnetic resonance imaging (MRI) scans of the bilateral hind limbs were respectively taken to document the perfusion-situation of the proximal and distal femoral artery (FA). 9.4 T scanner (Bruker BioSpec 94/20 AVIII, Bruker Biospin MRI GmbH, Ettlingen, Germany) as described in our previous research [45].

#### Functional evaluation and follow-up

To assess the functional recovery of the hind limb movement, mice were visually examined at the 0th, 1st, 3rd, 5th, and 7th days by functional scoring using the Tarlov scale as described previously [46, 47].

#### Plasma and tissue collection

The animals were sacrificed 7 days after the DLFA. Blood was collected from the inferior vena cava. Plasma was prepared by centrifuging the blood at 1000 rpm for 10 min at 4 °C and stored at -80 °C for biochemical analysis. Both sides of the fresh Vastus Lateralis (VL) and Gastrocnemius (GM) were rapidly removed after perfusion with 4% PFA and kept at -80 °C for further analysis.

#### Histological evaluation

The histological analysis of bilateral GM and aorta with Hematoxylin & Eosin (HE) and Immunohistochemistry (IHC) of CD31 and vWF staining were performed on all

mice as described in [45]. ImageJ software (version 1.52, Bethesda, USA) was used to estimate the percentage of the microvascular area (CD31 or vWF positive area) in randomly selected 5 fields of view ( $\times 40$ ).

To estimate the plaque burden in the vessels, the thoracoabdominal aorta was removed, fixed overnight in 4% PFA and paraffin-embedded sections (4  $\mu$ m) were derived. To determine the atherosclerotic burden (AS) in the artery, sections were stained for HE, and the progression stage of AS lesions were determined as previously described [48]. All the sections were inspected by conventional light microscopy.

#### Lactate dehydrogenase (LDH) assay

The relative levels of LDH in the VL tissue were detected using an LDH kit (Abcam, Germany, ab197000) following the manufacturer's guidelines. Briefly, 40 mg tissue was homogenized using a T18 digital homogenizer (IKA, USA) at the speed of  $2.5 \times 10^4$  rpm for 30 s in protein isolation buffer containing 20 mM Tris-HCl, 150 mM NaCl, 5 mM EDTA, 1% Triton X-100, 0.5% sodium deoxycholate, 1  $\mu$ M dithiothreitol (DTT), protease and phosphatase inhibitors and incubated on ice for 10 min. Tissue lysates were subsequently centrifuged for 5 min at 4 °C at  $1 \times 10^5$  g. Supernatant samples were collected and added to 96-well-plate (50  $\mu$ L each well). Hereafter, a 50  $\mu$ L reaction mix supplied by the kit was added to each sample and the fluorescence intensity at 535/587 nm (Ex/Em) was immediately measured using a Tecan multimode microplate reader.

#### Myoglobin (Mb) ELISA

Mouse Mb sandwich ELISA Kit (Abcam, Germany, ab210965) was used to determine levels of Mb in the VL tissue lysate according to the manufacturer's protocol. Briefly, 50  $\mu$ L of tissue lysate (previously described in the LDH assay) followed by 50  $\mu$ L of the Antibody Cocktail was added to each well of the 96-well-plate and incubated at room temperature for 1 h on a shaker (400 rpm). Afterward, the plate was washed thrice with 350  $\mu$ L of wash buffer. 100  $\mu$ L of 3,3',5,5'-Tetramethylbenzidine development solution was then added to each well and the plate was incubated for 10 min in dark. Finally, the stop solution was added (50  $\mu$ L each well) and optical density was measured at 450 nm on a multimode microplate reader.

#### Cholesterol, triglycerides and creatine kinase in plasma

Cholesterol, triglycerides and creatine kinase (CK) were determined in the plasma of each mouse using Cobas 311 analyzers (Roche, Switzerland). The analysis was performed as per the manufacturer's protocol.

### Western blot (WB)

Protein expression was determined by performing WB. Total protein isolated from the HUVECs and mice hind limb GM were mixed with loading buffer (Bio-Rad, Germany, 161-0767) and distilled water to obtain a concentration of 1  $\mu\text{g}/\mu\text{L}$  and denatured by incubation at 100 °C for 10 min. The denatured protein (25  $\mu\text{g}$ ) was loaded on the 10% SDS-PAGE acrylamide gels and then electrophoresed at 230 V for 1 h. Protein samples were transferred onto polyvinylidene fluoride membranes (PVDF, Bio-Rad, Germany, 1620177) by using a Turbo blot (Bio-Rad, Germany). Hereafter, the PVDF membrane was blocked for 1 h in Tris-buffered saline with 0.1% Tween 20 (TBST) containing 5% nonfat milk. Membranes were then incubated overnight at 4 °C with primary antibodies. After the incubation with primary antibodies, the PVDF membrane was washed with TBST and subsequently incubated for 1 h at room temperature with the corresponding HRP-conjugated secondary antibody. The detection of immune reactive bands was performed by enhanced luminol reagent and visualized by chemiluminescence (1–5 min exposure, Western Lightning Plus-ECL, PerkinElmer, USA, 203-17431). For detecting the phosphorylation of PLN, the PVDF membrane was stripped and re-probed. Densitometric analysis was performed with ImageJ software version 1.52.

### Statistical analysis

Statistical analyses were performed using SPSS 19.0 (IBM Corp., Armonk, USA) and GraphPad Prism 8 (GraphPad Software, USA). Results for the different experimental groups were expressed as mean  $\pm$  SD. To determine the optimal concentration of  $\text{CoCl}_2$ , DFO, TG, Ion and  $\text{H}_2\text{O}_2$  for use in the in vitro cell experiments regression analysis was performed by GraphPad Prism 8 to calculate their  $EC_{50}$  and  $IC_{50}$ . The differences between groups were analyzed by one-way or two-way analysis of variance (ANOVA) followed by Tukey's post hoc correction analysis and  $\chi^2$  test. We regarded the experimental results (such as microvascular density (MVD), LDH, Mb, CK, protein expression level, etc.) from the left hind limb (non-ischemic side) as the internal control to normalize the levels of relative results of every mouse. Throughout

the analysis,  $p$ -values  $< 0.05$  were considered statistically significant.

### Results

#### ABCB5<sup>+</sup> MSCs alleviate the overloading of Cyto Ca<sup>2+</sup> in hypoxic HUVECs

To investigate the relationship between extracellular  $\text{Ca}^{2+}$  and Cyto  $\text{Ca}^{2+}$  under hypoxia, SERCA2a inhibition and ROS, HUVECs were first treated by  $\text{CoCl}_2$ , DFO, TG,  $\text{H}_2\text{O}_2$  and the non-selective calcium ionophore Ion in HHBSS buffer without  $\text{Ca}^{2+}$  for 2 h. None of the treatments except for  $\text{H}_2\text{O}_2$  (Fig. 1D,  $P_{\text{H}_2\text{O}_2} = 0.9977$ ), led to a significant change of the Fura-2 ratio when cells were in HHBSS buffer without  $\text{Ca}^{2+}$  medium compared to non-treated cells (Fig. 1A,  $P_{\text{CoCl}_2} = 0.9484$ , Fig. 1B,  $P_{\text{DFO}} = 0.7792$ , Fig. 1C,  $P_{\text{TG}} = 0.9752$ ,  $P_{\text{Ion}} = 0.9355$ ). In the following 2 h, when the HHBSS buffer with  $\text{Ca}^{2+}$  was used keeping other conditions same, the Fura-2 ratio significantly increased (Fig. 1A,  $P_{\text{CoCl}_2} = 0.0034$ , Fig. 1B,  $P_{\text{DFO}} = 0.0002$ , Fig. 1C,  $P_{\text{TG}} < 0.0001$ , Fig. 1D,  $P_{\text{H}_2\text{O}_2} < 0.0001$ ,  $P_{\text{Ion}} < 0.0001$ ). This indicate extracellular  $\text{Ca}^{2+}$  influx leading to an increase in Cyto  $\text{Ca}^{2+}$  concentration, which is in line with the previous studies [22, 23].

Incubation with  $\text{CoCl}_2$  and DFO in cell culture medium lead to a significant increase in Cyto  $\text{Ca}^{2+}$  indicated by an increase in Fura-2 ratio as compared to the non-treated control HUVECs after 2 h of treatment (Fig. 1E,  $P_{(\text{CoCl}_2 \text{ vs. control})2\text{h}} < 0.0001$ , Fig. 1F,  $P_{(\text{DFO vs. control})2\text{h}} < 0.0001$ ). Afterward, the addition of MSC-CM or the introduction of MSC-CO, in the continued presence of  $\text{CoCl}_2$  or DFO, led to a slow decrease in the Fura-2 ratio over the following 24 h resembling the Fura-2 ratio of non-treated cells. Although both treatment modalities—conditioned medium as well as co-culture were successful in restoring Cyto  $\text{Ca}^{2+}$  level similar to that observed in control HUVECs, the MSC-CM treatment led  $\text{CoCl}_2$  or DFO treated HUVECs to reach this level in 12 and 16 h faster in comparison to MSC-CO (Fig. 1E,  $P_{(\text{CoCl}_2 \text{ vs. control})16\text{h}} = 0.5350$ ,  $P_{(\text{CoCl}_2\text{-CO vs. control})16\text{h}} = 0.2418$ , Fig. 1F,  $P_{(\text{DFO-CM vs. control})12\text{h}} = 0.6651$ ,  $P_{(\text{DFO-CO vs. control})12\text{h}} = 0.2625$ ). Addition of TG, ionomycin as well as  $\text{H}_2\text{O}_2$  also lead to increase in Cyto  $\text{Ca}^{2+}$  (Fig. 1G,  $P_{\text{TG}} < 0.0001$ , Fig. 1H,  $P_{\text{H}_2\text{O}_2} < 0.0001$ ,

(See figure on next page.)

**Fig. 1** ABCB5<sup>+</sup> MSCs alleviate overloading of Cyto  $\text{Ca}^{2+}$  in hypoxic HUVECs. **A–D** HUVECs loaded with 2  $\mu\text{M}$  Fura-2-acetoxymethyl ester (Fura 2-AM, Biotium, USA, 50033) were treated with **A** 80  $\mu\text{M}$   $\text{CoCl}_2$ ; **B** 120  $\mu\text{M}$  DFO; **C** 3  $\mu\text{M}$  TG; **D** 100  $\mu\text{M}$   $\text{H}_2\text{O}_2$  in HHBSS buffer without  $\text{Ca}^{2+}$  for 2 h. After 2 h, buffer was changed to HHBSS (contains DFO,  $\text{CoCl}_2$  or TG) with  $\text{Ca}^{2+}$ . 100  $\mu\text{M}$  Ionomycin (Ion) was used as positive control. The ratio of the fluorescence-emission intensities at 535 nm (340/380 nm) was measured using a Tecan multimode microplate reader by alternating excitation wavelength between 340 and 380 nm. **E–G** HUVECs loaded with 2  $\mu\text{M}$  Fura 2-AM were treated with 80  $\mu\text{M}$   $\text{CoCl}_2$ , or 120  $\mu\text{M}$  DFO or 3  $\mu\text{M}$  TG and the 100  $\mu\text{M}$  Ion in medium for 4 h. Afterward, HUVECs were either co-cultured with ABCB5<sup>+</sup>MSCs ( $\text{CoCl}_2$ -CO; DFO-CO; TG-CO) or cultured in ABCB5<sup>+</sup> MSC-CM ( $\text{CoCl}_2$ -CM; DFO-CM, TG-CM) for 24 h. Changes in Fura-2 ratio in HUVECs under **E**  $\text{CoCl}_2$ ,  $\text{CoCl}_2$ -CM and  $\text{CoCl}_2$ -CO treatments; **F** DFO, DFO-CM and DFO-CO treatments; **G** TG, TG-CM and TG-CO treatments. **H** Changes in Fura-2 ratio in HUVECs treated by 100  $\mu\text{M}$  Ion and 100  $\mu\text{M}$   $\text{H}_2\text{O}_2$ . Data is represented as mean  $\pm$  SD,  $n = 3$  in each group, ns, not significant, \* $p < 0.05$ , \*\* $p < 0.01$ , \*\*\* $p < 0.001$ , \*\*\*\* $p < 0.0001$



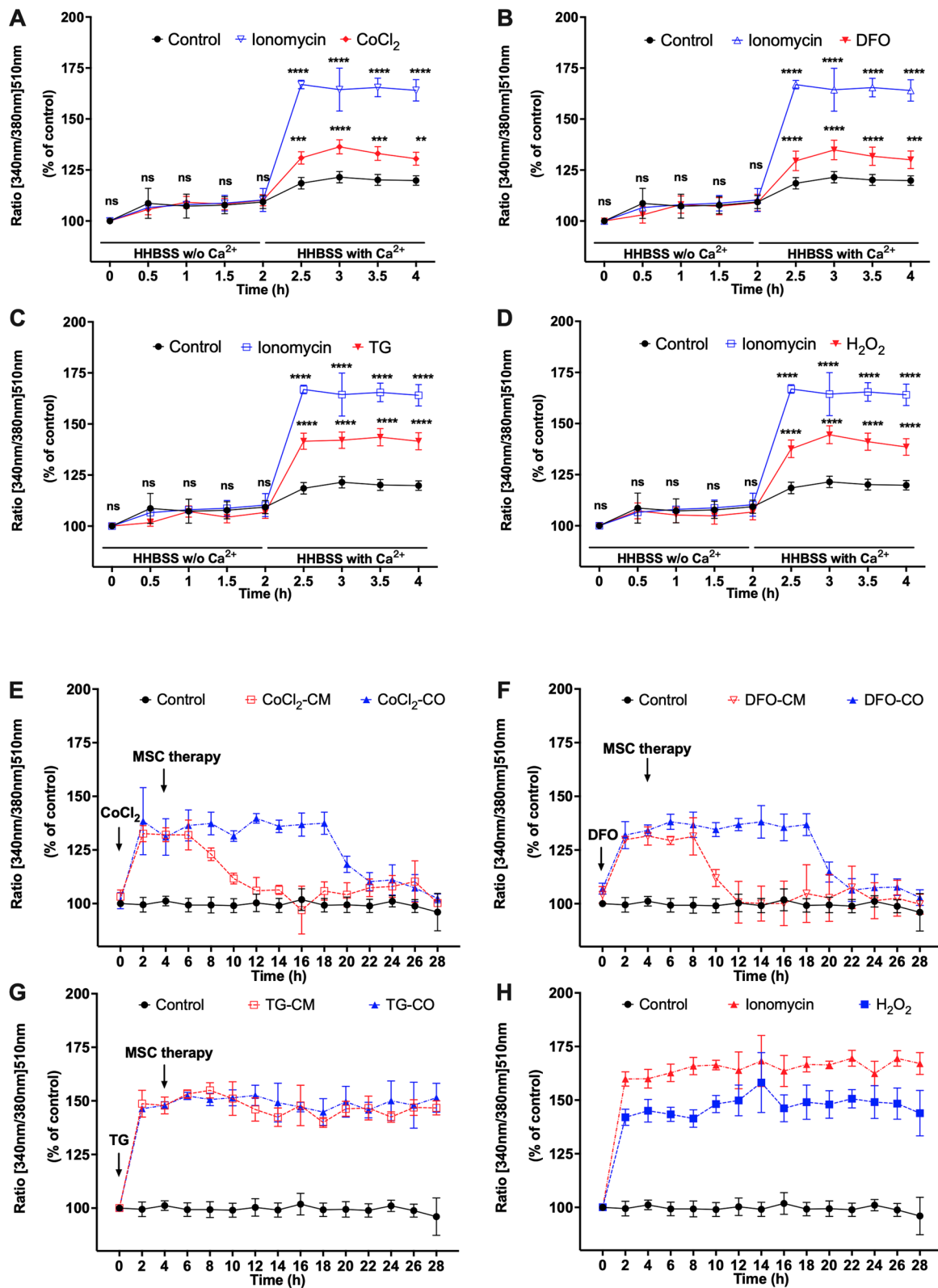


Fig. 1 (See legend on previous page.)

$P_{\text{Ion}} < 0.0001$ ). However, an additional MSC-CM or MSC-CO treatment did not change Cyto  $\text{Ca}^{2+}$  levels in the TG treatment group (Fig. 1G,  $P_{\text{TG-CM}} < 0.0001$ ,  $P_{\text{TG-CO}} < 0.0001$ ).

#### ABC $B5^+$ MSCs restore ER $\text{Ca}^{2+}$ in hypoxic HUVECs

To detect ER  $\text{Ca}^{2+}$  change in living HUVECs, the cells were transduced with the D1ER FRET sensor. After 4 h incubation with  $\text{CoCl}_2$ , DFO and TG, the FRET ratio in the all conditions significantly decreased compared to the non-treated control HUVECs (Fig. 2A,  $P_{\text{CoCl}_2} < 0.0001$ , Fig. 2B,  $P_{\text{DFO}} < 0.0001$ , Fig. 2C,  $P_{\text{TG}} = 0.0017$ , Fig. 2D,  $P_{\text{H}_2\text{O}_2} < 0.0001$ ). The decrease in ER  $\text{Ca}^{2+}$  induced by  $\text{CoCl}_2$  and DFO treatment was reversed by MSC-CM and MSC-CO treatment over the following 24 h (Fig. 2A,  $P_{(\text{CoCl}_2\text{-CM vs. control})10\text{h}} = 0.9877$ ,  $P_{(\text{CoCl}_2\text{-CO vs. control})20\text{h}} = 0.9409$ , Fig. 2B,  $P_{(\text{DFO-CM vs. control})6\text{h}} > 0.9999$ ,  $P_{(\text{DFO-CO vs. control})20\text{h}} = 0.1848$ ). Again, MSC-CM led to an earlier restoration of ER  $\text{Ca}^{2+}$  reversal than MSC-CO. After incubation with TG, the FRET ratio decreased (Fig. 2C,  $P_{(\text{TG vs. control})2\text{h}} = 0.0002$ ) and could not be reversed by MSC-CM or MSC-CO (Fig. 2C,  $P_{(\text{TG-CM vs. control})20\text{h}} < 0.0045$ ,  $P_{(\text{TG-CO vs. control})20\text{h}} = 0.0003$ ).  $\text{H}_2\text{O}_2$  treatment also significantly decreased the FRET ratio as compared to the control group (Fig. 2D,  $P_{(\text{H}_2\text{O}_2 \text{ vs. control})2\text{h}} < 0.0001$ ).

We also performed acceptor photo bleaching using fixed cell samples (Fig. 2E). Similar to the live cell experiments, here we also found that HUVECs treated with  $\text{CoCl}_2$ , DFO and TG displayed a significantly lower FRET ratio than the non-treated controls (Fig. 2F,  $P_{\text{CoCl}_2} < 0.0001$ , Fig. 2G,  $P_{\text{DFO}} < 0.0001$ , Fig. 2H,  $P_{\text{TG}} < 0.0001$ ). In the HUVECs treated with MSC-CM and MSC-CO treatment, the FRET ratio normalized back to the base line levels (Fig. 2F,  $P_{\text{CoCl}_2\text{-CM}} = 0.8491$ ,  $P_{\text{CoCl}_2\text{-CO}} = 0.9545$ , Fig. 2G,  $P_{\text{DFO-CM}} = 0.3504$ ,  $P_{\text{DFO-CO}} = 0.2102$ ). Again, MSC-CM and MSC-CO treatment were not effective in HUVECs treated with TG (Fig. 2H,  $P_{\text{TG-CM}} < 0.0001$ ,  $P_{\text{TG-CO}} = 0.0001$ ).

#### ABC $B5^+$ MSCs alleviated hypoxia-induced ROS burden in HUVECs

Hypoxia-mediated ROS formation can also interfere with  $\text{Ca}^{2+}$  homeostasis [49, 50]. Therefore, we next evaluated dynamic changes of ROS. To this end, roGFP3 expressing HUVECs were challenged with  $\text{CoCl}_2$  and DFO. A significant increase in ROS was observed in HUVECs incubated with  $\text{CoCl}_2$  and DFO in the first 4 h (Fig. 3A,  $P_{(\text{CoCl}_2 \text{ vs. control})4\text{h}} < 0.0001$ , Fig. 3B,  $P_{(\text{DFO vs. control})4\text{h}} < 0.0001$ ,  $P_{(\text{TG vs. control})4\text{h}} = 0.0017$ ). Incubation with  $\text{H}_2\text{O}_2$  (used as control) also led to a similar increase (Fig. 3A,  $P_{\text{H}_2\text{O}_2} < 0.0001$ ). Additional incubation with MSC-CM and MSC-CO reversed this increase in both  $\text{CoCl}_2$  and DFO groups in the following 24 h (Fig. 3A,  $P_{(\text{CoCl}_2\text{-CM vs. control})24\text{h}} = 0.9791$ ,  $P_{(\text{CoCl}_2\text{-CO vs. control})24\text{h}} = 0.8847$ , Fig. 3B,  $P_{(\text{DFO-CM vs. control})24\text{h}} = 0.2295$ ,  $P_{(\text{DFO-CO vs. control})24\text{h}} = 0.7574$ ). Here as well, MSC-CM was faster than MSC-CO to bring the ROS to basal level.

#### In-vitro ABC $B5^+$ MSCs restore ER $\text{Ca}^{2+}$ using the SERCA2a-PLN axis

Hypoxia and expression of HIF-1 $\alpha$  has been implicated in the suppression of SERCA2a expression [51]. Therefore, we assessed if this was also case in hypoxic HUVECs. WB results showed that incubation over 4 h with  $\text{CoCl}_2$ , DFO and  $\text{H}_2\text{O}_2$  led to a decrease in SERCA2a expression as compared to the control group (Fig. 4B,  $P_{\text{CoCl}_2} = 0.0042$ ,  $P_{\text{DFO}} = 0.0153$ ,  $P_{\text{H}_2\text{O}_2} = 0.0026$ ). When cells were incubated with MSC-CM and MSC-CO in addition to  $\text{CoCl}_2$ , SERCA2a expression increased to a similar level as the control group (Fig. 4B,  $P_{\text{CoCl}_2\text{-CM}} = 0.9193$ ,  $P_{\text{CoCl}_2\text{-CO}} = 0.9997$ ,  $P_{\text{DFO-CM}} = 0.9989$ ,  $P_{\text{DFO-CO}} = 0.9914$ ). The phosphorylation of PLN decreased significantly after incubation with  $\text{CoCl}_2$ , DFO and  $\text{H}_2\text{O}_2$  (Fig. 4D,  $P_{\text{CoCl}_2} = 0.0255$ ,  $P_{\text{DFO}} = 0.0287$ ,  $P_{\text{H}_2\text{O}_2} = 0.0005$ ). However, the ratio of pPLN/PLN under exposure of the cells with MSC-CM and MSC-CO did not change

(See figure on next page.)

**Fig. 2** ABC $B5^+$  MSCs restore ER  $\text{Ca}^{2+}$  in hypoxic HUVECs. **A–D** HUVECs transduced with the ratiometric ER- $\text{Ca}^{2+}$  sensor-D1ER, were treated with 80  $\mu\text{M}$   $\text{CoCl}_2$ , or 120  $\mu\text{M}$  DFO or 3  $\mu\text{M}$  TG for 4 h in medium. Thereafter, HUVECs were either co-cultured with ABC $B5^+$  MSCs ( $\text{CoCl}_2\text{-CO}$ ;  $\text{DFO-CO}$ ;  $\text{TG-CO}$ ) or cultured in ABC $B5^+$  MSC-CM ( $\text{CoCl}_2\text{-CM}$ ;  $\text{DFO-CM}$ ;  $\text{TG-CM}$ ) for 24 h. The ratio of CFP (Ex 430 nm/Em 474 nm) intensity by YFP (Ex 514 nm/Em 527 nm) intensity represented the dynamic changes in ER  $\text{Ca}^{2+}$  concentration and were measured using a Tecan multimode plate reader at every two hours. 100  $\mu\text{M}$  of  $\text{H}_2\text{O}_2$  was used as positive control. Changes in ER- $\text{Ca}^{2+}$  in HUVECs under **A**  $\text{CoCl}_2$ ,  $\text{CoCl}_2\text{-CM}$  and  $\text{CoCl}_2\text{-CO}$  treatments; **B** DFO,  $\text{DFO-CM}$  and  $\text{DFO-CO}$  treatments; **C** TG,  $\text{TG-CM}$  and  $\text{TG-CO}$  treatments; and **D**  $\text{H}_2\text{O}_2$  treatments. **E** Representative images of HUVECs under various treatments taken by SP5 microscopy system (scale bar is 200  $\mu\text{m}$ ). **F–H** D1ER expressing HUVECs were grown on 13 mm  $\varnothing$  glass coverslips treated with 80  $\mu\text{M}$   $\text{CoCl}_2$ , or 120  $\mu\text{M}$  DFO or 3  $\mu\text{M}$  TG in medium for 4 h. Subsequently, HUVECs were either co-cultured with ABC $B5^+$  MSCs ( $\text{CoCl}_2\text{-CO}$ ;  $\text{DFO-CO}$ ;  $\text{TG-CO}$ ) or cultured in ABC $B5^+$  MSC-CM ( $\text{CoCl}_2\text{-CM}$ ;  $\text{DFO-CM}$ ;  $\text{TG-CM}$ ) for 24 h and fixed with 4% PFA. Changes in ER- $\text{Ca}^{2+}$  in HUVECs under **F**  $\text{CoCl}_2$ ,  $\text{CoCl}_2\text{-CM}$  and  $\text{CoCl}_2\text{-CO}$  treatments; **G** DFO,  $\text{DFO-CM}$  and  $\text{DFO-CO}$  treatments; **H** TG,  $\text{TG-CM}$  and  $\text{TG-CO}$  treatments. Data is represented as mean  $\pm$  SD,  $n = 3$  in each group, ns, not significant, \* $p < 0.05$ , \*\* $p < 0.01$ , \*\*\* $p < 0.001$ , \*\*\*\* $p < 0.0001$

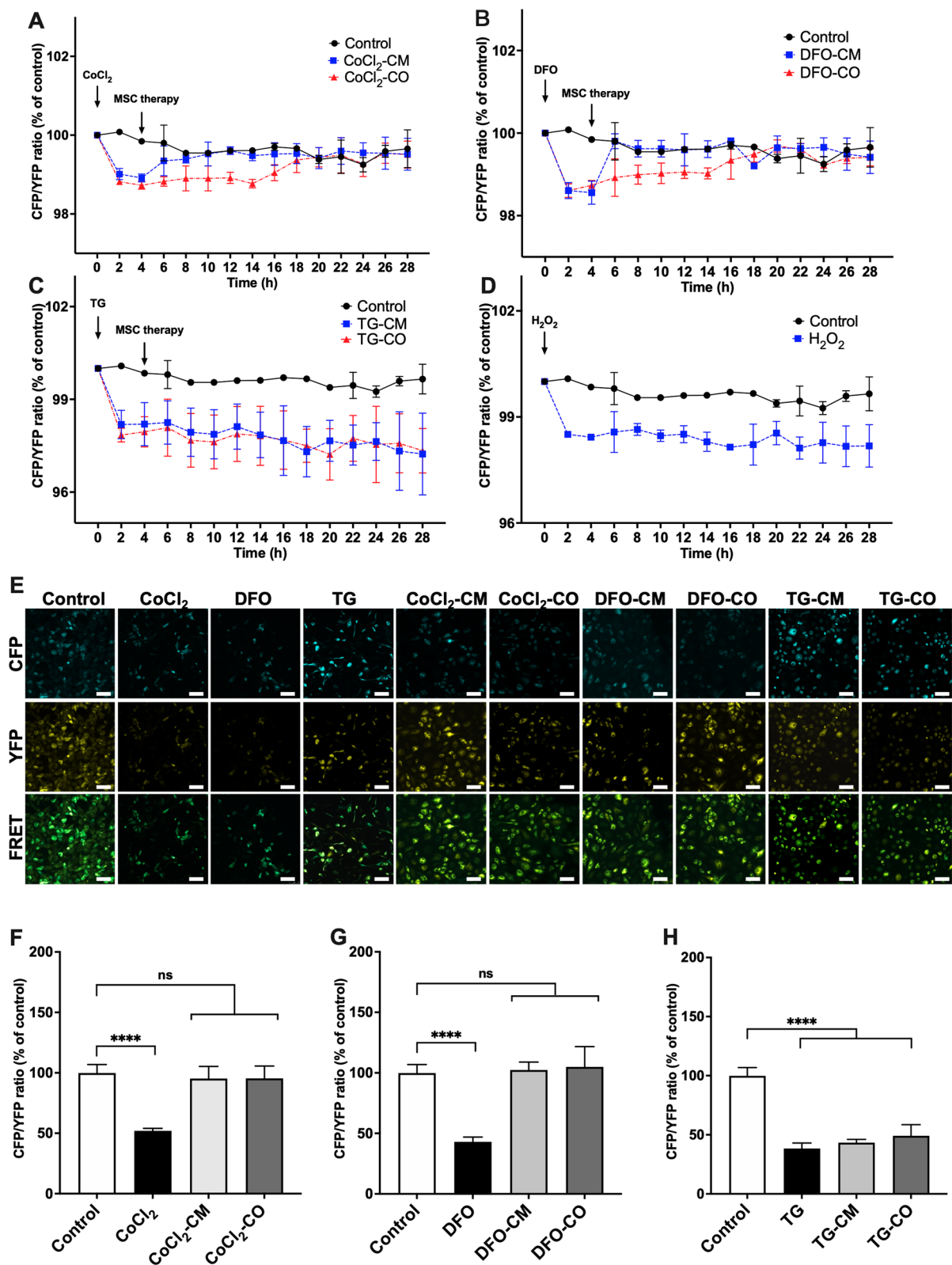
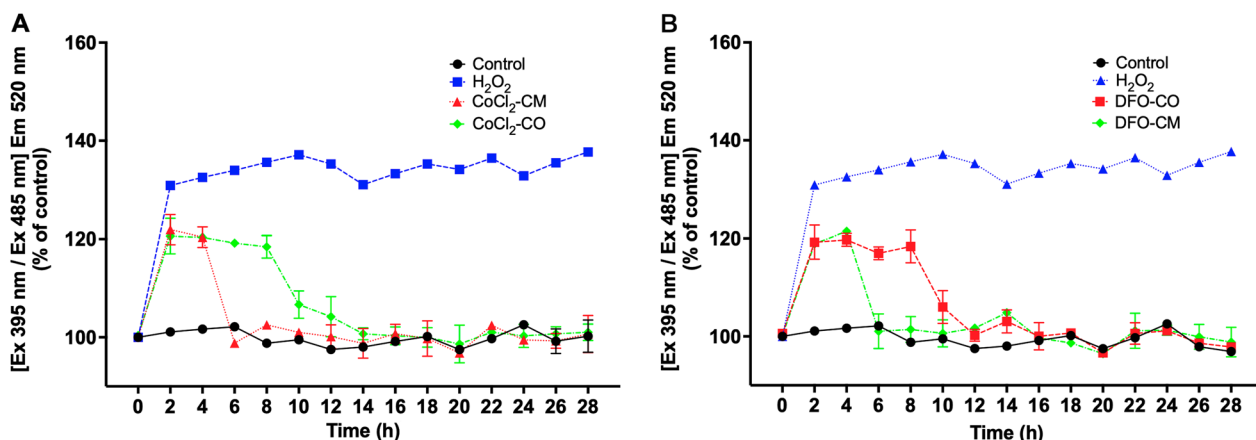
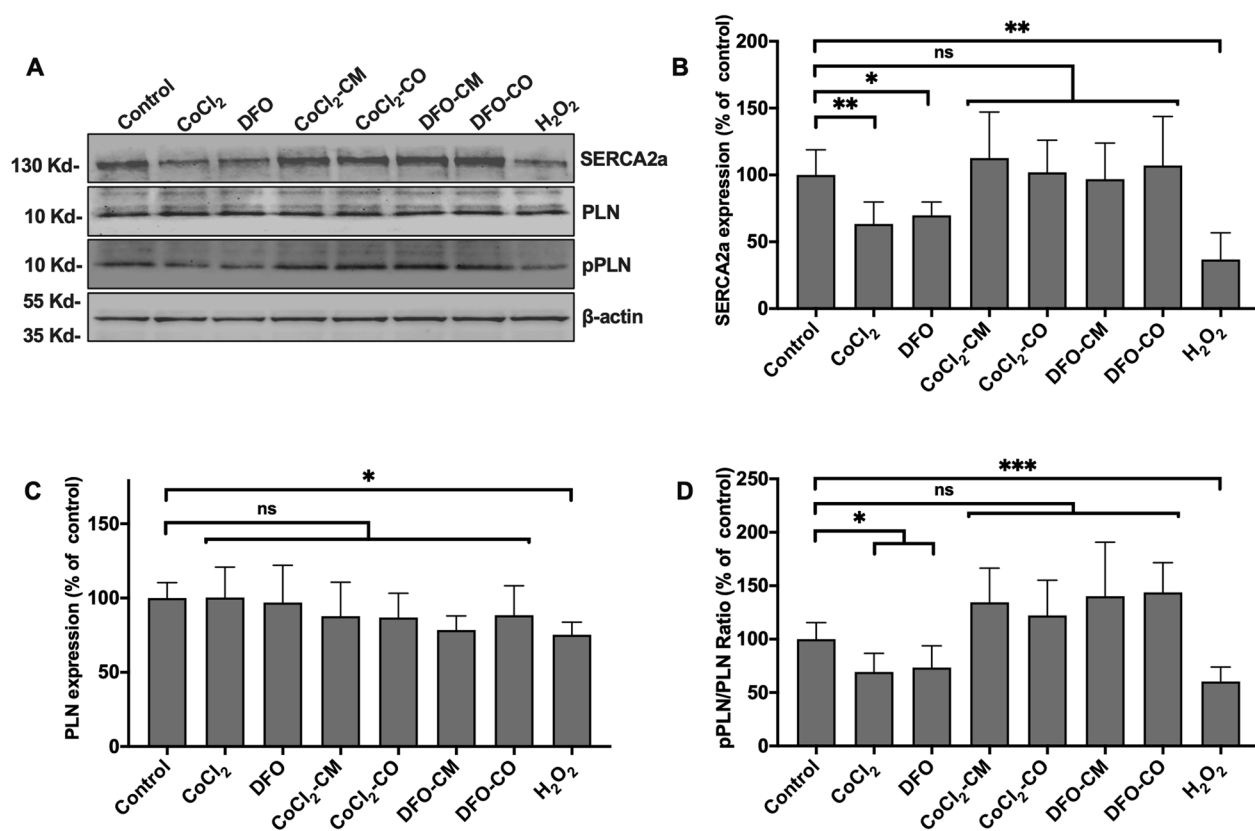


Fig. 2 (See legend on previous page.)



**Fig. 3** ABCB5<sup>+</sup> MSCs alleviated hypoxia-induced ROS burden in HUVECs. **A, B** HUVECs expressing roGFP3 were treated with 80  $\mu$ M CoCl<sub>2</sub>, or 120  $\mu$ M DFO or 100  $\mu$ M H<sub>2</sub>O<sub>2</sub> in medium for 4 h. H<sub>2</sub>O<sub>2</sub> was used as positive control. Thereafter, HUVECs were either co-cultured with ABCB5<sup>+</sup> MSCs (CoCl<sub>2</sub>-CO; DFO-CO) or cultured in ABCB5<sup>+</sup> MSC-CM (CoCl<sub>2</sub>-CM; DFO-CM) for 24 h. The ratio of florescence intensity Ex 395 nm and at Ex 485 nm, and the emission at 520 nm was measured by a Tecan multimode reader every 2 h and ratio was calculated. **A** ROS changes in HUVECs treated by CoCl<sub>2</sub>, CoCl<sub>2</sub>-CM and CoCl<sub>2</sub>-CO treatments; **B** DFO, DFO-CM and DFO-CO treatments. Data is represented as mean  $\pm$  SD, *n* = 3 in each group



**Fig. 4** In-vitro ABCB5<sup>+</sup> MSCs restore ER Ca<sup>2+</sup> using the SERCA2a-PLN axis. **A** The representative western blot showing SERCA2a, PLN, pPLN and  $\beta$ -actin expression in HUVECs under different treatments. **B–D** HUVECs were treated with 80  $\mu$ M CoCl<sub>2</sub>, or 120  $\mu$ M DFO or 100  $\mu$ M H<sub>2</sub>O<sub>2</sub> for duration of 4 h. Afterward, HUVECs were either co-cultured with ABCB5<sup>+</sup> MSCs (CoCl<sub>2</sub>-CO; DFO-CO) or cultured in ABCB5<sup>+</sup> MSC-CM (CoCl<sub>2</sub>-CM; DFO-CM) for 24 h. The expression of SERCA2a, PLN, Phosphorylated PLN (pPLN) and  $\beta$ -actin expression was determined by western blotting and quantified by densitometry using NIH ImageJ 1.52 software. Expression of SERCA2a and PLN is presented as fold change compared to untreated control cells while pPLN is shown as ratio of pPLN/PLN. Quantitative analysis of **B** SERCA2a, (normalized to  $\beta$ -actin) and **C** PLN expression (normalized to  $\beta$ -actin); and **D** ratio pPLN to PLN

significantly as compared to the control group (Fig. 4D,  $P_{\text{CoCl}_2\text{-CM}}=0.1827$ ,  $P_{\text{CoCl}_2\text{-CO}}=0.7414$ ,  $P_{\text{DFO-CM}}=0.5438$ ,  $P_{\text{DFO-CO}}=0.1840$ ).

#### **ABCB5<sup>+</sup> MSCs restore the angiogenic function of hypoxic HUVECs**

We evaluated the metabolic activity of HUVECs under chemically induced hypoxia upon treatment with CoCl<sub>2</sub> and DFO alone or in combination with MSC-CM and MSC-CO. CoCl<sub>2</sub> and DFO treatments significantly decreased HUVECs metabolic activity compared to controls (Fig. 5A,  $P_{\text{CoCl}_2}<0.0001$ , Fig. 5B,  $P_{\text{DFO}}<0.0001$ ). However, the MSC-CM and MSC-CO could counter the decrease in HUVECs metabolic activity (Fig. 5A,  $P_{\text{CoCl}_2\text{-CM}}=0.3758$ ,  $P_{\text{CoCl}_2\text{-CO}}=0.3666$ , Fig. 5B,  $P_{\text{DFO-CM}}=0.3005$ ,  $P_{\text{DFO-CO}}=0.0766$ ). To prove the influence of ER Ca<sup>2+</sup> store-depletion on the metabolic activity of HUVECs, the cells were also exposed to the SERCA inhibitor TG. Treatment of HUVECs with TG led to a further decrease in HUVECs metabolic activity (Fig. 5C,  $P_{\text{TG}}<0.0001$ ). Neither conditioned medium nor co-culture with ABCB5<sup>+</sup> MSCs were able to rescue HUVECs treated with TG (Fig. 5C,  $P_{\text{TG-CM}}<0.0001$ ,  $P_{\text{TG-CO}}<0.0001$ ).

Next, we evaluated if hypoxia affected HUVECs migratory properties using scratch assays (Fig. 5D). Indeed, the cell migration rate was reduced upon CoCl<sub>2</sub> or DFO treatment while incubation with TG led to an even more pronounced decrease in migration (Fig. 5E,  $P_{\text{CoCl}_2}<0.0001$ , Fig. 5F,  $P_{\text{DFO}}=0.0006$ , Fig. 5G,  $P_{\text{TG}}<0.0001$ ) compared with untreated HUVECs. Again, MSC-CM and MSC-CO were able to rescue the migration rate in HUVECs under hypoxia except when the treatments were combined with TG (Fig. 5E,  $P_{\text{CoCl}_2\text{-CM}}>0.9999$ ,  $P_{\text{CoCl}_2\text{-CO}}>0.9999$ , Fig. 5F,  $P_{\text{DFO-CM}}>0.9999$ ,  $P_{\text{DFO-CO}}>0.9999$ , Fig. 5G,  $P_{\text{TG-CM}}<0.0001$ ,  $P_{\text{TG-CO}}<0.0001$ ).

In the tube formation assays, HUVECs displayed the ability to form junctions and meshes automatically under normoxia (Fig. 6A). Under CoCl<sub>2</sub> and DFO treatment,

the number of meshes and junctions significantly reduced compared to untreated HUVECs (Meshes: Fig. 6B,  $P_{\text{CoCl}_2}=0.0124$ , Fig. 6C,  $P_{\text{DFO}}=0.0205$ , Junctions: Fig. 6B,  $P_{\text{CoCl}_2}=0.0003$ , Fig. 6C,  $P_{\text{DFO}}<0.0001$ ). Incubation with MSC-CM or MSC-CO counteracted this effect (Meshes: Fig. 6B,  $P_{\text{CoCl}_2\text{-CM}}=0.9939$ ,  $P_{\text{CoCl}_2\text{-CO}}=0.6444$ , Fig. 6C,  $P_{\text{DFO-CM}}=0.9566$ ,  $P_{\text{DFO-CO}}=0.9538$ , Junctions: Fig. 6B,  $P_{\text{CoCl}_2\text{-CM}}=0.8115$ ,  $P_{\text{CoCl}_2\text{-CO}}=0.8898$ , Fig. 6C,  $P_{\text{DFO-CM}}=0.9854$ ,  $P_{\text{DFO-CO}}=0.4850$ ). In the TG treated HUVECs, only few meshes and junctions were formed and neither MSC-CM nor MSC-CO restored the counteracted this effect (Fig. 6D, Meshes:  $P_{\text{TG}}<0.0001$ ,  $P_{\text{TG-CM}}<0.0001$ ,  $P_{\text{TG-CO}}<0.0001$ , Junctions:  $P_{\text{TG}}<0.0001$ ,  $P_{\text{TG-CM}}<0.0001$ ,  $P_{\text{TG-CO}}<0.0001$ ).

#### **ABCB5<sup>+</sup> MSCs decreased weight loss of ApoE<sup>-/-</sup> mice**

Double ligation of the femoral artery was performed to induce acute-on-chronic hypoxia in ApoE<sup>-/-</sup> mice that had been fed on a Western diet for 12 weeks. All 24 mice were successfully operated on. One day after the DLFA, MRI confirmed proximal and distal parts of the right FA were occluded (Fig. 7D). Although, two mice died in the control group on the 4th and 6th days after the procedure yet there was no significant difference in the survival rate of the control group and ABCB5<sup>+</sup> MSCs treated group (Fig. 7A,  $P=0.1351$ ). HE sections of the aorta showed atherosclerotic lesions (Additional file 4: Fig. S4A, B) and no differences were observed in the manifestation of aortic AS between both groups (Additional file 4: Fig. S4C,  $P=0.4652$ ). A comparison of cholesterol and triglycerides in the plasma of the two groups showed no significant differences (Additional file 4: Fig. S4D,  $P_{\text{Cholesterol}}=0.9176$ , Additional file 4: Fig. S4E,  $P_{\text{Triglycerides}}=0.8828$ ).

To understand the well-being of the mice changes in body weight were observed. Mice were weighed before the DLFA operation (Pre-DLFA) and 7 days after the DLFA operation (Post-DLFA). The mean Pre-DLFA weights of control and ABCB5<sup>+</sup> MSCs groups were  $34.5 \pm 2.5$  g and  $32.8 \pm 3.1$  g, respectively. There was no

(See figure on next page.)

**Fig. 5** ABCB5<sup>+</sup> conditioned medium and co-culture both rescue metabolic activity and migration properties of hypoxic HUVECs. **A–C** HUVECs were treated either with 80 μM CoCl<sub>2</sub> or 120 μM DFO for 4 h to induce hypoxia. HUVECs were also treated with 3 μM of TG. Afterward, HUVECs were either co-cultured with ABCB5<sup>+</sup> MSCs (CoCl<sub>2</sub>-CO; DFO-CO; TG-CO) or cultured in ABCB5<sup>+</sup> MSC conditioned medium (CoCl<sub>2</sub>-CM; DFO-CM; TG-CM) for 24 h. HUVECs without treatment served as control. Cellular metabolic activity of HUVECs was measured by MTT assay which is an indirect indicator of cell viability. HUVECs metabolic activity under **A** CoCl<sub>2</sub>, CoCl<sub>2</sub>-CM and CoCl<sub>2</sub>-CO treatments; **B** DFO, DFO-CM and DFO-CO treatments; **C** TG, TG-CM and TG-CO treatments. **D** Representative figure showing HUVECs migration under different treatments (scale bar is 200 μm). **E–G** Scratch assays were used to study migratory properties of HUVECs. After treatment with 80 μM CoCl<sub>2</sub> or 120 μM DFO or 3 μM TG for 4 h, HUVECs monolayer was scratched along a straight line. Afterward, HUVECs were either co-cultured with the ABCB5<sup>+</sup> cells (CoCl<sub>2</sub>-CO; DFO-CO; TG-CO) or cultured with ABCB5<sup>+</sup> conditioned medium (CoCl<sub>2</sub>-CM; DFO-CM; TG-CM). The photos of the monolayer were taken at 0 h, 6 h, 12 h, and 24 h by an inverted microscope (Axiovert 200 M; Zeiss, Jena, Germany). The gap area was quantitatively evaluated using NIH ImageJ software (version 1.52, Bethesda, USA). Migration rate of HUVECs under **E** CoCl<sub>2</sub>, CoCl<sub>2</sub>-CM and CoCl<sub>2</sub>-CO treatments; **F** DFO, DFO-CM and DFO-CO treatments; **G** TG, TG-CM and TG-CO treatments. Data is represented as mean ± SD,  $n=3$  in each group, ns, not significant, \* $p<0.05$ , \*\* $p<0.01$ , \*\*\* $p<0.001$ , \*\*\*\* $p<0.0001$

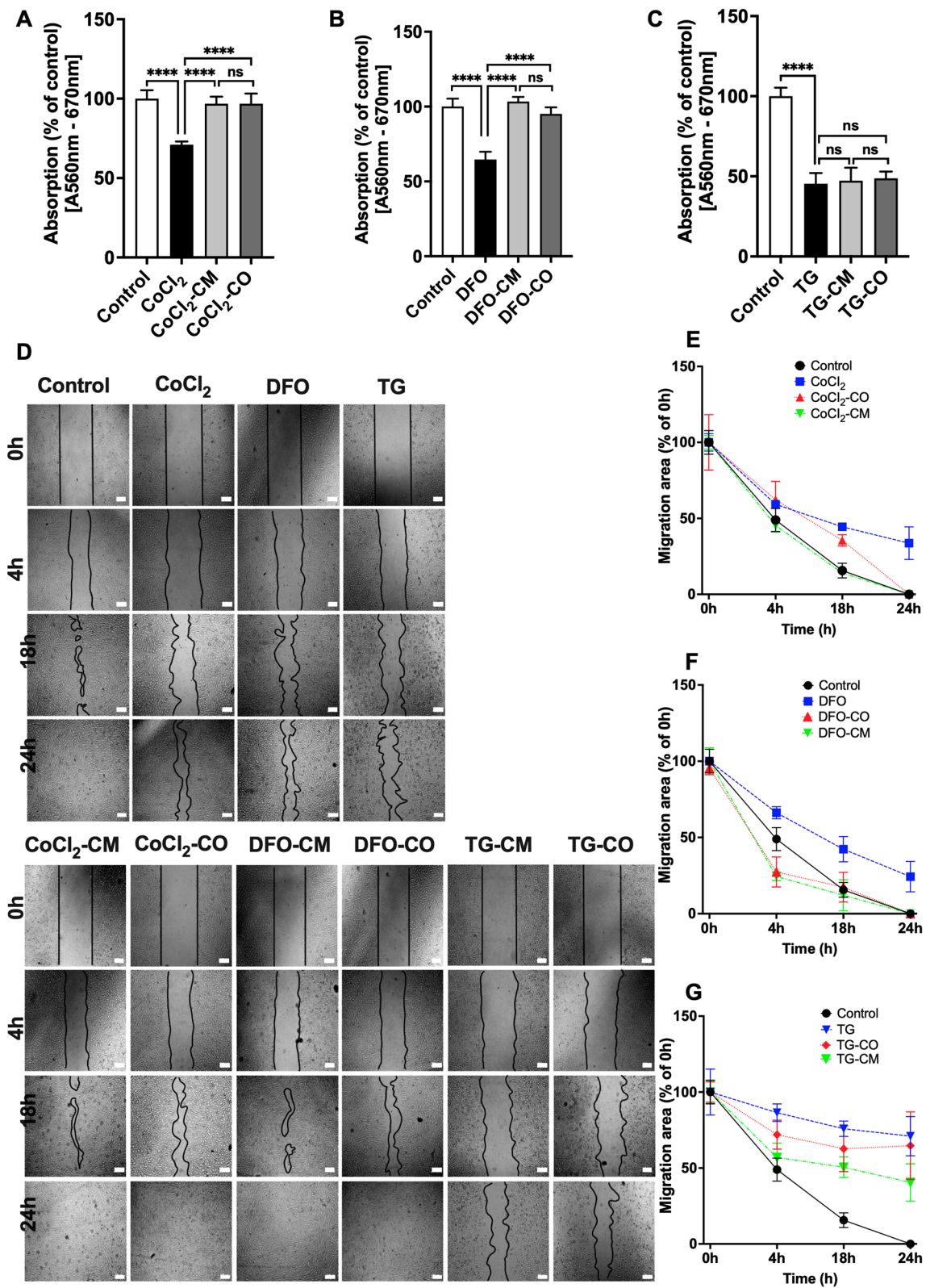
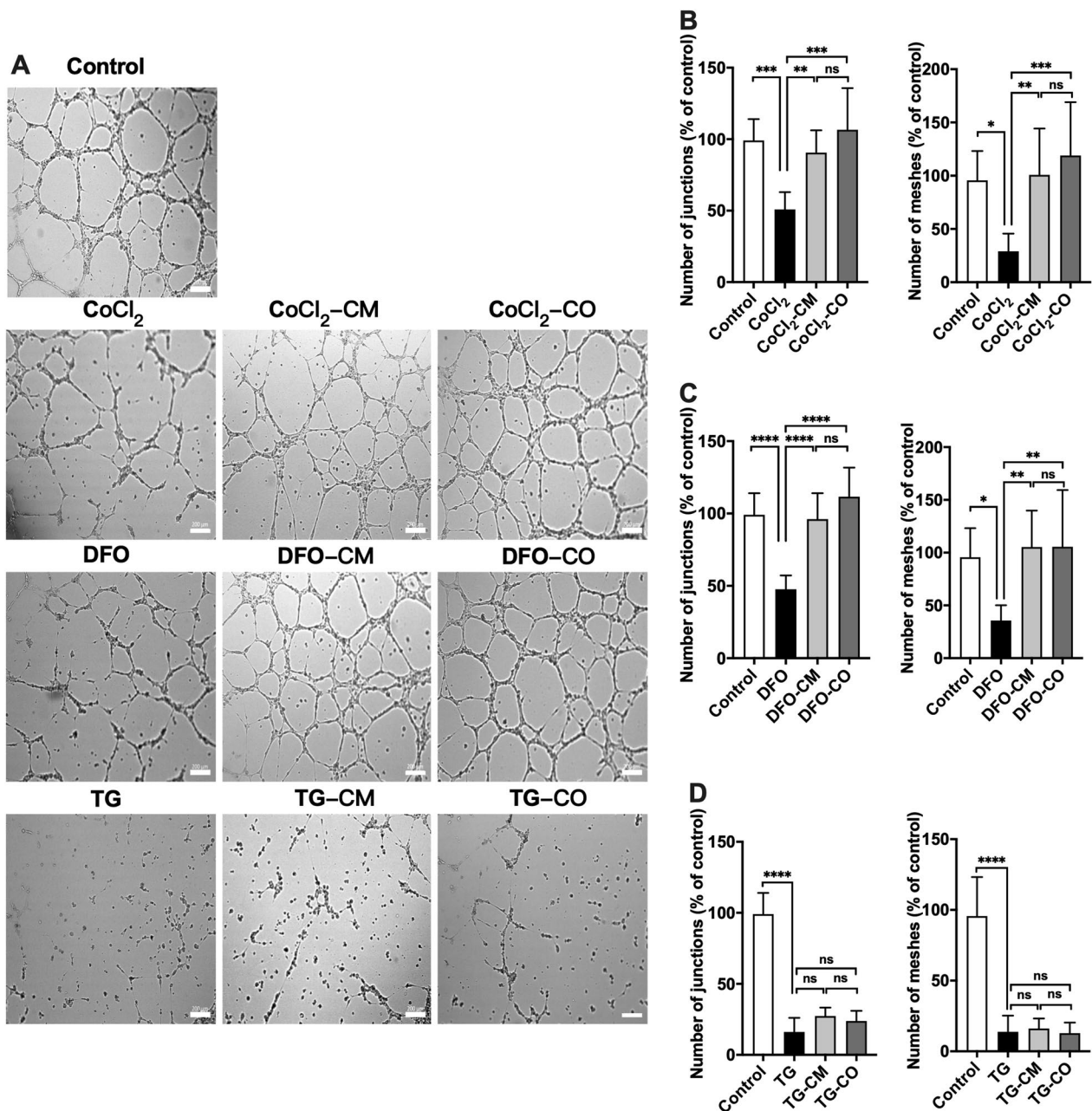


Fig. 5 (See legend on previous page.)



**Fig. 6** ABCB5<sup>+</sup> conditioned medium as well as co-culture rescue angiogenic properties of hypoxic HUVECs. **A** Representative images showing tube formation in HUVECs under different culture conditions (scale bar is 200 μm). **B–D** HUVECs were treated with 80 μM CoCl<sub>2</sub> or 120 μM DFO or 3 μM TG for 4 h. Then the HUVECs were harvested and seeded onto the growth factor reduced matrigel pre-coated 24-well plates (2.5 × 10<sup>4</sup> cells/well). Afterward HUVECs were either co-cultured with ABCB5<sup>+</sup> MSCs (CoCl<sub>2</sub>-CO; DFO-CO; TG-CO) or cultured in ABCB5<sup>+</sup> MSC conditioned medium (CoCl<sub>2</sub>-CM; DFO-CM; TG-CM). Images were taken by an inverted microscope (Axiovert 200 M; Zeiss, Jena, Germany) after 6 h of incubation. The number of HUVECs meshes and junctions were analyzed by the angiogenesis analyzer plugin for NIH ImageJ version 1.52. Meshes and junctions after incubation with **B** CoCl<sub>2</sub>, CoCl<sub>2</sub>-CM and CoCl<sub>2</sub>-CO treatments; **C** DFO, DFO-CM and DFO-CO treatments; **D** TG, TG-CM and TG-CO treatments. Data is represented as mean ± SD, *n* = 3 in each group, ns not significant, \**p* < 0.05, \*\**p* < 0.01, \*\*\**p* < 0.001, \*\*\*\**p* < 0.0001

significant difference in the Pre-DLFA weights between the two groups (Fig. 7B,  $P_{\text{Pre-DLFA}}=0.1295$ ). The mean weights of control and ABCB5<sup>+</sup> MSCs groups 7-day Post-DLFA were  $30.77 \pm 2.15$  g and  $30.67 \pm 3.73$  g, respectively. The comparison of 7-day Post-DLFA between the two groups also displayed no significant difference (Fig. 7B,  $P_{\text{Post-DLFA}}=0.9349$ ). However, the ABCB5<sup>+</sup> MSCs group

showed proportionally a significantly lower weight loss than the control group (Fig. 7B,  $P=0.0096$ ).

**ABCB5<sup>+</sup> MSCs improved functional recovery of ApoE<sup>-/-</sup> mice after hind limb ischemia**

The motoric function of mice was determined after DLFA using Tarlov Scale. The scores decreased significantly on the 1st day after the DLFA operation in both

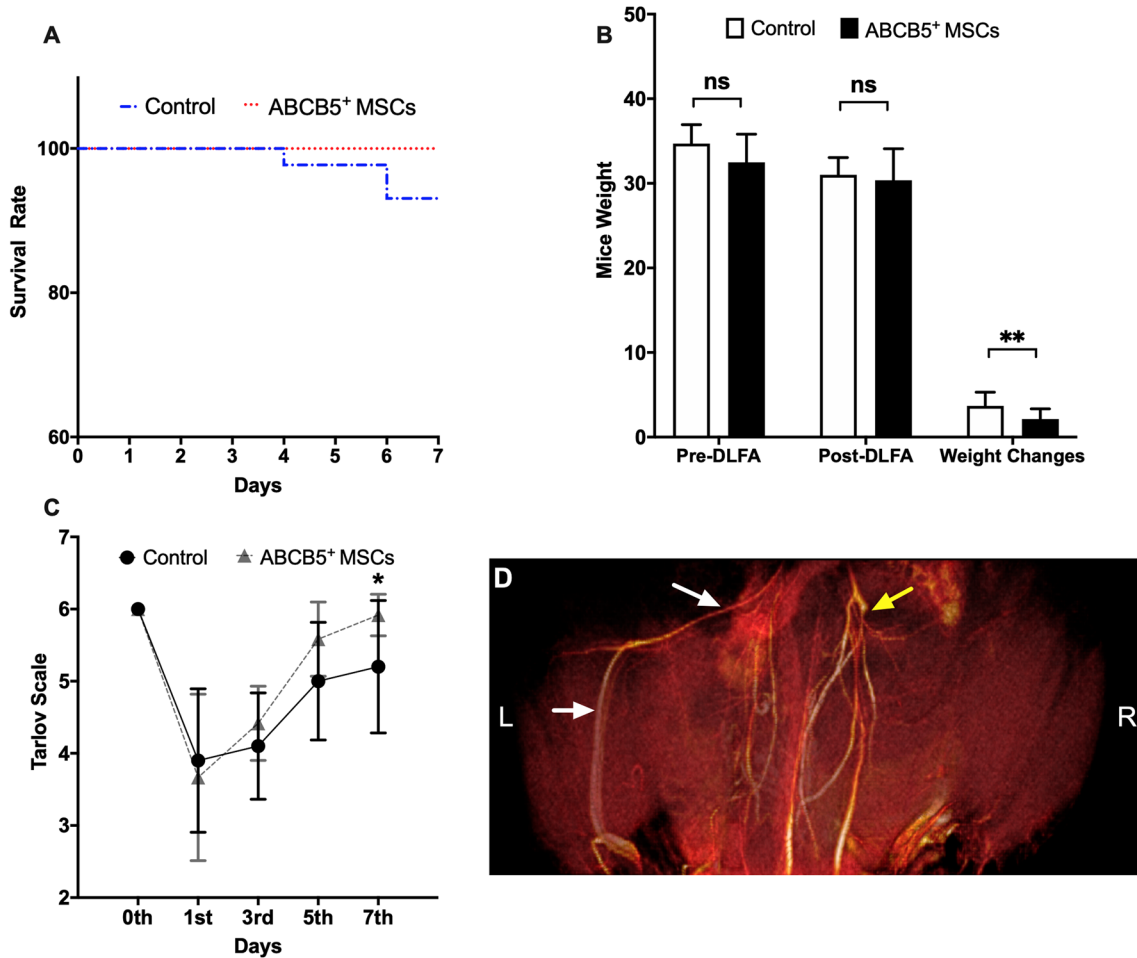


**Fig. 7** ABCB5<sup>+</sup> cells therapy in ApoE<sup>-/-</sup> mice after DLFA leads to reduced weight loss. **A** The survival rate of ApoE<sup>-/-</sup> mice after DLFA and receiving ABCB5<sup>+</sup> MSCs (ABCB5<sup>+</sup> MSCs) or saline (control) treatment ( $n=12$  in each group). **B** Body weight of each of the animals was assessed directly prior to induction of DLFA and 7 days thereafter. **C** Tarlov Scale changes before and 7 days after induction of DLFA. **D** A representative MRI scan after the DLFA operation (scale bar: 5 mm). The right femoral artery (FA) was blocked (yellow arrow) as compared to the left FA (white arrow). Data were represented as mean  $\pm$  SD,  $n=12$  in ABCB5<sup>+</sup> MSCs group,  $n=12$  in controls group, ns, not significant, \* $p < 0.05$ , \*\* $p < 0.01$ , \*\*\* $p < 0.001$

(See figure on next page.)

**Fig. 8** ABCB5<sup>+</sup> MSCs therapy improve microvascular density in ApoE<sup>-/-</sup> mice after DLFA. **A, C** Representative pictures of IHC staining for **A** CD31 and **B** vWF (black arrow) in bilateral gastronemicus muscles (GM) of the ABCB5<sup>+</sup> MSCs treated as well as control mice (scale bar: 200  $\mu$ m). **B, D** Comparison of the ratio of **B** CD31 and **D** vWF positive areas in GM sections of ischemic and non-ischemic hindlimbs between control and ABCB5<sup>+</sup> MSCs groups. **E** LDH ratios levels in VL tissues derived from controls and the ABCB5<sup>+</sup> MSCs group; **F** Mb ratios level in VL tissues derived from both groups. Data were represented as mean  $\pm$  SD,  $n=10$  in ABCB5<sup>+</sup> MSCs group,  $n=12$  in controls group, ns, not significant, \* $p < 0.05$ , \*\* $p < 0.01$ , \*\*\* $p < 0.001$ , \*\*\*\* $p < 0.0001$



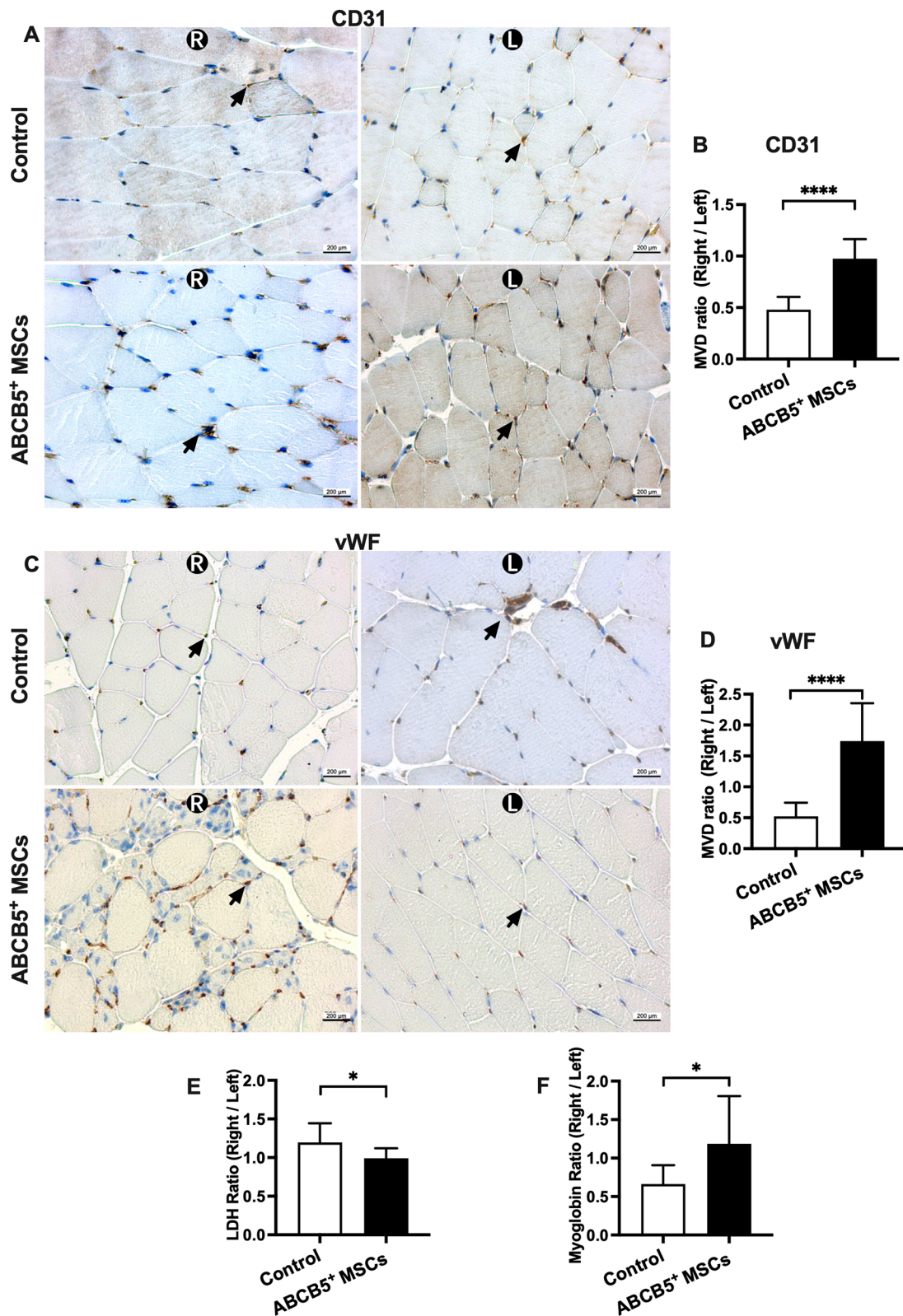


**Fig. 8** (See legend on previous page.)

groups and then increased within the following days. The average functional recovery was similar in the ABCB5<sup>+</sup> MSCs treated and the control group on the 3rd and the 5th day. However, ABCB5<sup>+</sup> MSCs treated mice display better motor functions compared to the saline-treated control mice on the 7th day (Fig. 7C, *P* = 0.0185). We did not observe any necrosis or gangrenous tissue after DLFA on the hind limb in any of the mice.

**ABCB5<sup>+</sup> MSCs therapy improved MVD in ApoE<sup>-/-</sup> mice after hind limb ischemia**

The ratio of CD31 positive areas in GM sections of ischemic and non-ischemic hind limbs was significantly higher in the ABCB5<sup>+</sup> MSCs group as compared to the control group (Fig. 8A, B, *P* < 0.0001). As another kind of marker of ECs, the ratio of vWF positive areas in the ABCB5<sup>+</sup> MSCs group was also significantly higher than in the control group (Fig. 8C, D, *P* < 0.0001). These results indicated that MVD in the ABCB5<sup>+</sup> MSCs group was

higher than in the control group and the ABCB5<sup>+</sup> MSC therapy displayed a peri-angiogenic effect.

**LDH and Mb in the hind limb muscle**

The ratio of LDH enzyme levels in VL tissues of ischemic hind limbs and non-ischemic hind limbs was used to determine muscle damage post DLFA between the two groups. In the ABCB5<sup>+</sup> MSC group, LDH ratios were significantly lower than in the control group (Fig. 8E, *P* = 0.0200). The Mb ratios of the ABCB5<sup>+</sup> MSC group were significantly higher than those in the control group (Fig. 8F, *P* = 0.0210).

**SERCA2a and pPLN in hind limb muscle samples**

WB was performed to measure expression levels of SERCA2a, PLN and pPLN in GM tissue samples (Fig. 9A, B). The ratio (ischemic/non-ischemic) of SERCA2a expression in ABCB5<sup>+</sup> MSCs group showed no significant difference (Fig. 9C, *P* = 0.1014). The phosphorylation of PLN in muscle specimens derived from animals of the ABCB5<sup>+</sup> MSCs group showed a significantly higher ratio

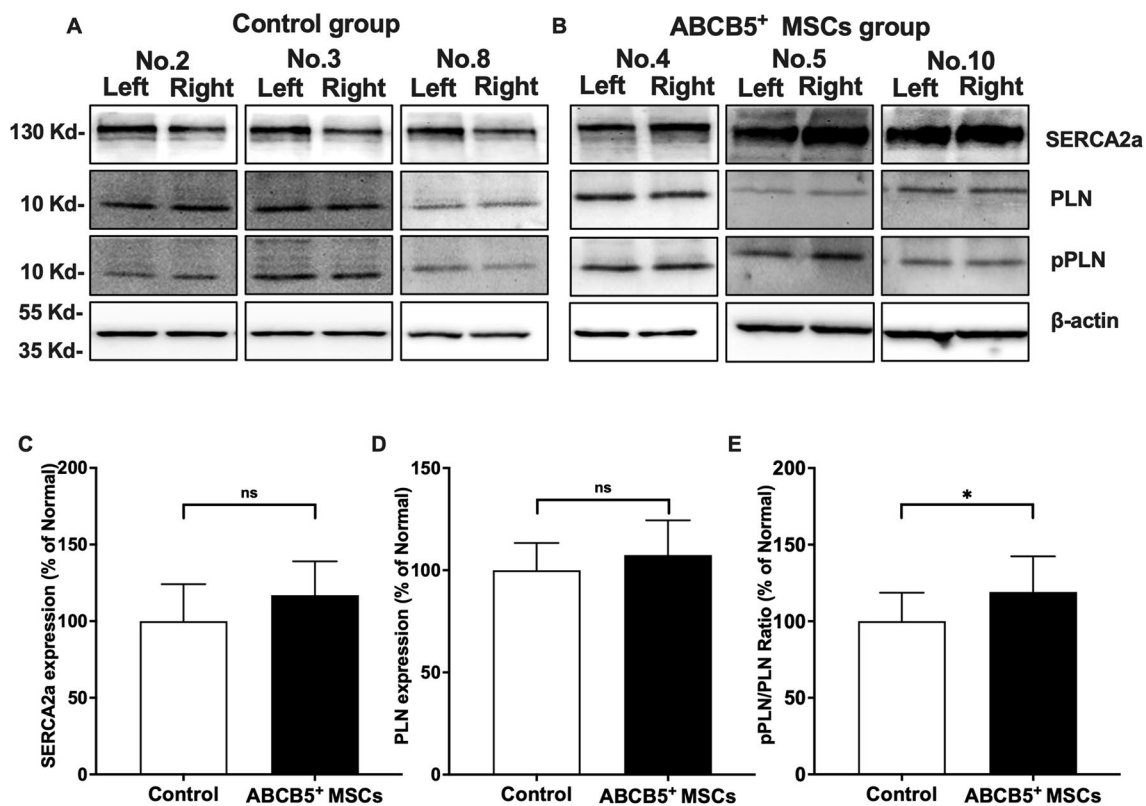


**Fig. 9** In-vivo ABCB5<sup>+</sup> MSCs restore ER Ca<sup>2+</sup> using the SERCA2a-PLN axis. **A, B** Representative SERCA2a, PLN, pPLN, and β-actin expression in bilateral gastrocnemius muscle (GM) samples from the 3 mice from control (**A**) and ABCB5<sup>+</sup> MSC treated groups (**B**). Full-length blots are presented in Additional file 5: Fig. S5. **C–E** Densitometric quantification of **C** SERCA2a expression (normalized to left side), **D** PLN expression (normalized to left side) and **E** pPLN/PLN (normalized to left side). Data were represented as mean ± SD, *n* = 10 control and *n* = 12 in ABCB5<sup>+</sup> MSCs group, ns, not significant, \**p* < 0.05

(ischemic/non-ischemic) as compared to the control group (Fig. 9E,  $P=0.0484$ ).

## Discussion

Hypoxia under physiological conditions stimulates angiogenesis [3–5]. However, under pathological circumstances as observed in cerebral ischemia, myocardial infarction and PAD [6, 7], prolonged hypoxia also perturbs  $\text{Ca}^{2+}$  homeostasis, oxidative stress and cellular apoptosis leading to end organ damage. Although the benefits of some stem cell therapies for PAD have been discussed previously, the influence of ABCB5<sup>+</sup> MSCs on ECs  $\text{Ca}^{2+}$  homeostasis (which is essential for angiogenesis [34]) remains to be determined.

In this study, we have demonstrated firstly, in an in-vitro model, that hypoxia leads to Cyto  $\text{Ca}^{2+}$  increase and ER  $\text{Ca}^{2+}$  depletion in HUVECs and that MSC-CM or MSC-CO can alleviate this effect. Secondly, we show that MSC-CM or MSC-CO also eliminates hypoxia-mediated ROS stress. Thirdly, we describe that MSC-CM and MSC-CO restore hypoxia perturbed ER- $\text{Ca}^{2+}$  via modulation of the expression of SERCA2a and the phosphorylation of PLN. Fourthly, ABCB5<sup>+</sup> MSCs restore the angiogenic function of hypoxic HUVECs. Finally, we show that ABCB5<sup>+</sup> MSCs therapy improves MVD and reduced damage to the hind limb muscles in ApoE<sup>-/-</sup> mice under hind limb ischemia.

As an irreversible inhibitory reagent of SERCA2a, TG could irreversibly bind to the SERCA2a to decrease the ER restoring ability. The results of our research also show that the treatment of TG significantly lead to the ER  $\text{Ca}^{2+}$  decreasing and Cyto  $\text{Ca}^{2+}$  increasing. Besides, the experimental results also show that the metabolic activity, migration rate and the tube formation ability of the HUVECs were all significantly decreased under the TG treatment. It demonstrated that the ER  $\text{Ca}^{2+}$  restoring ability played an important role in the angiogenic function of HUVECs.

Under hypoxia induced by treatment of HUVECs with  $\text{CoCl}_2$  and DFO, an increase in Cyto  $\text{Ca}^{2+}$  and ER  $\text{Ca}^{2+}$  liberation was observed. Long-term hypoxia as observed in PAD leads to depletion of cellular ATP. ATP is required by several pumps and ion transporters to maintain a  $\text{Ca}^{2+}$  gradient not just within various organelles in the cells but also between the cell and the extracellular environment [52]. Dysfunction of these pumps and ion transporters due to ATP exhaustion caused by hypoxia leads to an influx of extracellular  $\text{Ca}^{2+}$  and store-depletion of ER  $\text{Ca}^{2+}$ . This in turn activates plasma membrane  $\text{Ca}^{2+}$  channels, leading to an influx of  $\text{Ca}^{2+}$  into the cytosol resulting in a Cyto  $\text{Ca}^{2+}$  overload [22, 23, 53] which affects ECs cellular function, as we observed with a significant decrease in metabolic activity, migration rate

and reduced number of meshes and junctions in hypoxic HUVECs as compared to the control groups. These perturbations in the normal cellular function of the HUVECs also affect the ECs angiogenic function [54, 55]. Co-culture with ABCB5<sup>+</sup> MSCs or in ABCB5<sup>+</sup> MSCs condition medium restored both cytoplasmic as well as ER  $\text{Ca}^{2+}$  to the pre-hypoxia levels and exerted a restorative effect on metabolic activity and angiogenic function. Although both co-culture and condition medium reversed the effect of hypoxia yet faster recovery was observed in hypoxic HUVECs cultured in ABCB5<sup>+</sup> MSCs conditioned medium. MSCs secrete different paracrine factors under hypoxia and hyperoxia (21%  $\text{O}_2$ ) [56], whether ABCB5<sup>+</sup> MSCs also exhibit such change remains for further investigations.

Treatment of HUVECs with  $\text{CoCl}_2$  and DFO leads to a decrease in the expression of SERCA2a as well as in the PLN phosphorylation rate. This was also observed when HUVECs were treated with only  $\text{H}_2\text{O}_2$ , suggesting the role of hypoxia-induced mitochondrial ROS. Indeed, SERCA2a expression has been shown to decrease significantly under hypoxia. This may be induced either by low oxygen concentration [57] or  $\text{CoCl}_2$  treatment [58], which also leads to an increase in ROS. Physiological levels of ROS lead to the formation of glutathione adducts from S-glutathione and SERCA2a in both whole muscle tissue as well as in ECs which maintain the  $\text{Ca}^{2+}$  store in ER [59, 60]. This is essential for VEGF-induced  $\text{Ca}^{2+}$  influx and migration which has a direct consequence on angiogenic signaling [59, 60]. Under pathological conditions. ROS causes excessive oxidation of the cysteine residues in SERCA, resulting in decreased Cyto  $\text{Ca}^{2+}$  uptake, thus depleting the ER  $\text{Ca}^{2+}$  stores and causing dysregulated downstream signaling. For instance, SERCA2a activity in myocardium derived from infarction sites is attenuated due to the decrease of phosphorylation of PLN [61–64]. It is already known that accumulated ROS in ECs derails  $\text{Ca}^{2+}$  homeostasis that potentially resulting in cell death and even end-organ tissue damage [6, 29, 65]. Co-culture with ABCB5<sup>+</sup> MSCs or culture in ABCB5<sup>+</sup> MSCs condition medium restored SERCA2a expression and the phosphorylation ratio of PLN in hypoxic HUVECs. This can be attributed to the anti-oxidative effect exerted by MSCs and MSC-CM. Previous studies have reported that the stem cell exerts ROS suppression in a variety of in vitro and in vivo models of disease [66–71]. MSCs and MSC-CM are known to directly scavenge free radicals, bolster endogenous antioxidant defenses [72] and deliver functional mitochondria via extracellular vesicles [73]. This subsequently explains the restorative effect of ABCB5 MSCs and their conditioned medium on SERCA2a expression in hypoxic HUVECs.

Mice receiving ABCB5<sup>+</sup> MSCs treatment after DLFA exhibited less muscle damage suggested by significantly less release of LDH, and Mb in the GM and VL muscle tissue and improved MVD. Functional recovery after DLFA determined by applying the Tarlov Scale is consistent with the previous reports [74]. Correspondingly to the in vitro WB results, in vivo in the GM muscle lysate, we observed a higher pPLN/PLN ratio in mice receiving ABCB5<sup>+</sup> MSCs than in the saline-treated control group. However, no difference in the expression level of SERCA2a was observed between ABCB5<sup>+</sup> MSCs treated mice and controls. The main reason may be that the hind limb not only contains ECs and that other cell types might express a different isoform of SERCA.

We identified some potential limitations in this research. The first limitation is our recent results still could not provide enough evidence to completely elucidate the mechanism of the ABCB5<sup>+</sup> MSCs therapeutic effect on Ca<sup>2+</sup> homeostasis of HUVECs under the hypoxia. Maybe the hypoxia-driven changes in the Ca<sup>2+</sup> homeostasis of HUVECs may also have an effect on the cell biology of the ABCB5<sup>+</sup> MSCs which could interact again with the HUVECs. So the interaction of ABCB5<sup>+</sup> MSCs and ECs under hypoxic still needs to be explored. Secondly, because the current assays utilized are only applicable in vitro, the research project didn't mention the Ca<sup>2+</sup> homeostasis on the ischemic injury. In vivo, we only focused on the protective effect of the ABCB5<sup>+</sup> MSCs in a model of acute on chronic ischemia. More experiments needed be planned to establish the direct relationship between ABCB5<sup>+</sup> MSCs, Ca<sup>2+</sup> homeostasis, and protection from ischemia injury in the future. Finally, although the majority of Cyto Ca<sup>2+</sup> is eliminated by SERCA2a (74%), Cyto Ca<sup>2+</sup> is also eliminated via alternative ways such as the Na<sup>+</sup>/Ca<sup>2+</sup> exchanger (24%), the sarcolemmal Ca<sup>2+</sup> ATPase (1%) and the mitochondrial uniporter (1%) [75]. It remains uncertain how much of the ER Ca<sup>2+</sup> restoring ability is mediated by SERCA2a and PLN. Here knock-down experiments using siRNA to silence SERCA2a will be helpful in further research.

## Conclusion

In vitro, we demonstrated that the hypoxia can functionally impair the ER Ca<sup>2+</sup> restoring ability by inducing downregulation of SERCA2a expression and PLN phosphorylation in HUVECs, which then disrupts the ER Ca<sup>2+</sup> homeostasis and hereby perturbs the angiogenic function. We further suggest that ROS may play a role in this process. ABCB5<sup>+</sup> MSCs therapy could restore the homeostasis of ER Ca<sup>2+</sup> and Cyto Ca<sup>2+</sup> by increasing

SERCA2a expression and the phosphorylation of PLN, hereby enhancing the angiogenic function of ECs under hypoxia in vitro and under hind limb ischemia in vivo. This provides new evidence of a protective effect of ABCB5<sup>+</sup> MSCs in ischemia and supports the application of ABCB5<sup>+</sup> MSCs for novel therapeutic approaches in the future.

## Abbreviations

PAD	Peripheral artery disease
ECs	Endothelial cells
ABCB5 <sup>+</sup> MSCs	ATP-binding cassette subfamily B member 5 positive mesenchymal stromal cells
VEGF	Vascular endothelial growth factor
ROS	Reactive oxygen species
HIF	Hypoxia-inducible factor
ER	Endoplasmic reticulum
Cyto	Cytosolic
SERCA2a	Sarco-/endoplasmic reticulum ATPase 2a
PLN	Phospholamban
ApoE <sup>-/-</sup>	Apolipoprotein E knock-out
HUVECs	Human umbilical cord vein endothelial cells
vWF	Willebrand factor
FBS	Fetal bovine serum
P/S	Penicillin and streptomycin
CoCl <sub>2</sub>	Cobalt (II) chloride
DFO	Deferoxamine
TG	Thapsigargin
ABCB5 <sup>+</sup> MSC-CO	ATP-binding cassette subfamily B member 5 positive mesenchymal stromal cell coculture
ABCB5 <sup>+</sup> MSC-CM	ATP-binding cassette subfamily B member 5 positive mesenchymal stromal cell conditioned medium
MTT	3-(4, 5-Dimethyl thiazolyl)-2, 5-diphenyltetrazolium bromide
DMSO	Dimethyl sulfoxide
SDS	Sodium dodecyl sulfate
FRET	Fluorescence resonance energy transfer
YFP	Yellow fluorescent protein
CFP	Cyan fluorescent protein
PFA	Paraformaldehyde
Fura 2-AM	Fura-2-acetoxymethyl ester
H <sub>2</sub> O <sub>2</sub>	Hydrogen peroxide
Ion	Ionomycin
S.C.	Subcutaneous injection
DLFA	Double ligation of the right femoral artery
MRI	Magnetic resonance imaging
FA	Femoral artery
VL	Vastus lateralis
GM	Gastrocnemius
HE	Hematoxylin & Eosin
IHC	Immunohistochemistry
AS	Atherosclerosis
LDH	Lactate dehydrogenase
DTT	Dithiothreitol
Mb	Myoglobin
CK	Creatine kinase
WB	Western blot
PVDF	Polyvinylidene fluoride
TBST	Tris-buffered saline with 0.1% Tween 20
ANOVA	Analysis of variance
MVD	Microvascular density
Pre-DLFA	Before the DLFA operation
Post-DLFA	After the DLFA operation

## Supplementary Information

The online version contains supplementary material available at <https://doi.org/10.1186/s13287-022-03228-w>.

**Additional file 1: Figure S1.** Dose and kinetics of  $\text{CoCl}_2$ . HUVECs were treated with different concentration of  $\text{CoCl}_2$  for different duration of time and HIF-1 $\alpha$  expression levels was evaluated via western blotting. **A** A representative WB showing HIF-1 $\alpha$  expression levels in HUVECs. HIF-1 $\alpha$  increased in a dose-dependent manner after incubation with  $\text{CoCl}_2$  for 4 h. Regression analysis of densitometric quantification yielded an  $EC_{50}$  of 15.68  $\mu\text{M}$ . **B** A representative WB displaying that HIF-1 $\alpha$  expression increased in a time-dependent fashion under 100  $\mu\text{M}$   $\text{CoCl}_2$  treatment and peaked at 4 h of treatment and stayed steady until 24 h. **C** HUVECs transduced with roGFP3 displayed an increase in ROS signal when subjected to increasing concentration of  $\text{CoCl}_2$ . Regression analysis indicated that  $EC_{50}$  for ROS under  $\text{CoCl}_2$  treatment was 80.33  $\mu\text{M}$ . Response to 100  $\mu\text{M}$   $\text{H}_2\text{O}_2$  was noted as maximum ROS response (100%) and was used to normalize response obtained upon  $\text{CoCl}_2$  treatment. **D** HUVECs metabolic activity measured via MTT, decreased with increasing  $\text{CoCl}_2$  concentration. An  $IC_{50}$  of 126.7  $\mu\text{M}$  was determined by regression analysis. Data were represented as mean  $\pm$  SD,  $n=3$ , ns, not significant,  $*p<0.05$ .

**Additional file 2: Figure S2.** Dose and kinetics of DFO. HUVECs were treated with different concentrations of DFO for 4 h and HIF-1 $\alpha$  expression levels was evaluated using western blots (WB). **A** A representative WB showing that HIF-1 $\alpha$  expression increased in a dose-dependent manner under incubation with DFO and regression analysis indicated an  $EC_{50}$  of 63.68  $\mu\text{M}$ . **B** HIF-1 $\alpha$  expression levels increased time-dependently under 100  $\mu\text{M}$  DFO. Its expression level significantly increased after 2 h and reached a plateau at 4 h of DFO treatment. **C** HUVECs transduced with roGFP3 displayed an increase in ROS signal when subjected to increasing concentration of DFO. Regression analysis revealed the  $EC_{50}$  to be 121.9  $\mu\text{M}$ . Response to 100  $\mu\text{M}$   $\text{H}_2\text{O}_2$  was noted as maximum ROS response (100%) and was used to normalize responses obtained for DFO treatment. **D** A decrease in the metabolic activity of HUVECs which corresponded to the increase of DFO concentration was observed in MTT assay. An  $IC_{50}$  of 169.7  $\mu\text{M}$  was determined by regression analysis. Data were represented as mean  $\pm$  SD,  $n=3$ , ns, not significant,  $*p<0.05$ .

**Additional file 3: Figure S3.**  $IC_{50}$  of Thapsigargin (TG), Hydrogen Peroxide ( $\text{H}_2\text{O}_2$ ), and Ionomycin (Ion). HUVECs were subjected to different concentrations of TG,  $\text{H}_2\text{O}_2$  and Ion for 4 h and MTT assay was performed. **A** HUVECs metabolic activity decreased with the increase of TG concentrations. Regression analysis was performed and  $IC_{50}$  of TG on HUVECs was found to be 3417 nM. **B** HUVECs metabolic activity also decreased with the increase of  $\text{H}_2\text{O}_2$  concentrations. Regression analysis showed  $IC_{50}$  of  $\text{H}_2\text{O}_2$  on HUVECs to be 131.3  $\mu\text{M}$ . **C** HUVECs metabolic activity decreased with the increasing concentrations of Ion. Regression analysis yielded the  $IC_{50}$  of Ion on HUVECs as 117.4  $\mu\text{M}$ . Data were represented as mean  $\pm$  SD,  $n=3$ , ns, not significant,  $*p<0.05$ .

**Additional file 4: Figure S4.** No significant difference was observed in AS lesions, cholesterol, triglycerides between ABCB5 $^+$  MSC treated and untreated mice. 7 days post DLFA, blood and aorta samples from mice were taken. A representative HE stained sections of the aorta from the **A** control group and **B** ABCB5 $^+$  MSC treated mice. A1 and B1 displays atherosclerotic vessel wall while A2 and B2 displays normal vessel wall (scale bar is 50  $\mu\text{m}$  in Figure A and B; and 200  $\mu\text{m}$  in Figure A1, A2, B1, B2). **C** Comparison of aortic AS lesion appearance between ABCB5 $^+$  MSC treated and control mice. **D** Triglyceride concentration and **E** Cholesterol concentration in plasma between two groups of mice. Data were represented as mean  $\pm$  SD,  $n=10$  in ABCB5 $^+$  MSCs group,  $n=12$  in controls group, ns, not significant.

**Additional file 5: Figure S5.** Full-length blots. **A, B** Full-length blots of SERCA2a, PLN, pPLN, and  $\beta$ -actin expression in left (L) and right (R) sides from control (A) and ABCB5 $^+$  MSC treated groups (B).

## Acknowledgements

We thank Prof. Dr. Frank Zoellner for helping us to do the MRI scan, Dr. med. vet. Bettina Kränzlin, Dipl. Ing. Ina Schaefer for the introduction of confocal

microscopy system, Silke Deiters for the introduction of HE staining, Camela Jost, Maria Muciek for help with the plasma detection and Viktoria Skude for her valuable support and inputs with the animal surgery. We acknowledge the support of the Microscopy Core Facility Mannheim at the Medical Faculty Mannheim.

## Author contributions

KY, JZ, LL, PP and MK conducted the experiments, collected and analyzed the data, and prepared the manuscript; KY and JZ established the animal models; PP, MAK, BY, MK, RM, CG provided the technical and writing guidance; KY, JZ, LL and PP collected the data; MK, SV, RM, MHF and PP designed the experiments, supervised the whole work, and approved the final version of the manuscript. All authors read and approved the final manuscript.

## Funding

Open Access funding enabled and organized by Projekt DEAL. This study was supported by TICEBA GmbH.

## Availability of data and materials

The datasets used and analyzed during the current study are available from the corresponding author on reasonable request.

## Declarations

### Ethics approval and consent to participate

The protocol of HUVECs isolation was approved by the local ethics committee (Ethikkommission II der Medizinische Fakultät Mannheim AZ 2015-518N-MA). All experimental procedures were performed according to the EC guideline EC 2010/63/EU and have been approved by the local German legislation (35-9185.81/G[1]239/18). 8-week-old male ApoE $^{-/-}$  mice with the C57BL/6J background were purchased from Charles River Laboratories.

### Consent for publication

Not applicable.

### Competing interests

MAK is CSO of TICEBA GmbH, the manufacturer of the ABCB5 $^+$  MSCs. Remaining authors declare no competing interests.

### Author details

<sup>1</sup>Department of Surgery, Medical Faculty Mannheim, Heidelberg University, Mannheim, Germany. <sup>2</sup>European Center of Angioscience (ECAS), Medical Faculty Mannheim, Heidelberg University, Mannheim, Germany. <sup>3</sup>TICEBA GmbH, Heidelberg, Germany. <sup>4</sup>RHEACELL GmbH & Co. KG, Heidelberg, Germany. <sup>5</sup>V Department of Medicine, Medical Faculty Mannheim, Heidelberg University, Mannheim, Germany. <sup>6</sup>Department for General and Visceral Surgery, Theresienkrankenhaus Mannheim, Mannheim, Germany. <sup>7</sup>Department of Dermatology, Brigham and Women's Hospital, Harvard Medical School, Boston, MA, USA. <sup>8</sup>Transplant Research Program, Boston Children's Hospital, Harvard Medical School, Boston, MA, USA. <sup>9</sup>Harvard Stem Cell Institute, Harvard University, Cambridge, MA, USA. <sup>10</sup>School of Medical and Health Sciences, Edith Cowan University, Perth, WA, Australia. <sup>11</sup>Department of Surgery, University Hospital Mannheim, Theodor-Kutzer-Ufer 1-3, 68161 Mannheim, Germany.

Received: 14 March 2022 Accepted: 21 December 2022

Published online: 09 February 2023

## References

- Annex BH, Cooke JP. New directions in therapeutic angiogenesis and arteriogenesis in peripheral arterial disease. *Circ Res.* 2021;128:1944–57.
- Bahadori B, Uitz E, Mayer A, Harauer J, Dam K, Truschig-Wilders M, et al. Polymorphisms of the hypoxia-inducible factor 1 gene and peripheral artery disease. *Vasc Med.* 2010;15:371–4.
- Phillips PG, Birnby LM, Narendran A. Hypoxia induces capillary network formation in cultured bovine pulmonary microvessel endothelial cells. *Am J Physiol.* 1995;268:789–800.
- Tandara AA, Mustoe TA. Oxygen in wound healing—more than a nutrient. *World J Surg.* 2004;28:294–300.

5. Manalo DJ, Rowan A, Lavoie T, Natarajan L, Kelly BD, Ye SQ, et al. Transcriptional regulation of vascular endothelial cell responses to hypoxia by HIF-1. *Blood*. 2005;105:659–69.
6. Wong BW, Marsch E, Treps L, Baes M, Carmeliet P. Endothelial cell metabolism in health and disease: impact of hypoxia. *EMBO J*. 2017;36:2187–203.
7. Carmeliet P, Jain RK. Principles and mechanisms of vessel normalization for cancer and other angiogenic diseases. *Nat Rev Drug Discov*. 2011;10:417–27.
8. Behroozian A, Beckman JA. Microvascular disease increases amputation in patients with peripheral artery disease. *Arterioscler Thromb Vasc Biol*. 2020;40:534–40.
9. Robbins JL, Jones WS, Duscha BD, Allen JD, Kraus WE, Regensteiner JG, et al. Relationship between leg muscle capillary density and peak hyperemic blood flow with endurance capacity in peripheral artery disease. *J Appl Physiol*. 1985;2011(111):81–6.
10. Szabo GV, Kovess Z, Cserepes J, Daroczy J, Belkin M, Acsady G. Peripheral blood-derived autologous stem cell therapy for the treatment of patients with late-stage peripheral artery disease—results of the short- and long-term follow-up. *Cytotherapy*. 2013;15:1245–52.
11. Tateishi-Yuyama E, Matsubara H, Murohara T, Ikeda U, Shintani S, Masaki H, et al. Therapeutic angiogenesis for patients with limb ischaemia by autologous transplantation of bone-marrow cells: a pilot study and a randomised controlled trial. *Lancet*. 2002;360:427–35.
12. Xie B, Luo H, Zhang Y, Wang Q, Zhou C, Xu D. Autologous stem cell therapy in critical limb ischemia: a meta-analysis of randomized controlled trials. *Stem Cells Int*. 2018;2018:7528464.
13. Gao W, Chen D, Liu G, Ran X. Autologous stem cell therapy for peripheral arterial disease: a systematic review and meta-analysis of randomized controlled trials. *Stem Cell Res Ther*. 2019;10:140.
14. Peeters Weem SM, Teraa M, de Borst GJ, Verhaar MC, Moll FL. Bone marrow derived cell therapy in critical limb ischemia: a meta-analysis of randomized placebo controlled trials. *Eur J Vasc Endovasc Surg*. 2015;50:775–83.
15. Ballikaya S, Sadeghi S, Niebergall-Roth E, Nitzl L, Frindert J, Norrick A, et al. Process data of allogeneic ex vivo-expanded ABCB5(+) mesenchymal stromal cells for human use: off-the-shelf GMP-manufactured donor-independent ATMP. *Stem Cell Res Ther*. 2020;11:482.
16. Kerstan A, Niebergall-Roth E, Esterlechner J, Schroder HM, Gasser M, Waaga-Gasser AM, et al. Ex vivo-expanded highly pure ABCB5(+) mesenchymal stromal cells as Good Manufacturing Practice-compliant autologous advanced therapy medicinal product for clinical use: process validation and first in-human data. *Cytotherapy*. 2021;23:165–75.
17. Vander Beken S, de Vries JC, Meier-Schiesser B, Meyer P, Jiang D, Sindrilari A, et al. Newly defined ATP-binding cassette subfamily b member 5 positive dermal mesenchymal stem cells promote healing of chronic iron-overload wounds via secretion of interleukin-1 receptor antagonist. *Stem Cells*. 2019;37:1057–74.
18. Schatton T, Yang J, Kleffel S, Uehara M, Barthel SR, Schlapbach C, et al. ABCB5 identifies immunoregulatory dermal cells. *Cell Rep*. 2015;12:1564–74.
19. Jiang D, Muschhammer J, Qi Y, Kugler A, de Vries JC, Saffarzadeh M, et al. Suppression of neutrophil-mediated tissue damage—a novel skill of mesenchymal stem cells. *Stem Cells*. 2016;34:2393–406.
20. Semenza GL. HIF-1: mediator of physiological and pathophysiological responses to hypoxia. *J Appl Physiol*. 1985;2000(88):1474–80.
21. Semenza GL. Regulation of mammalian O<sub>2</sub> homeostasis by hypoxia-inducible factor 1. *Annu Rev Cell Dev Biol*. 1999;15:551–78.
22. Arnould T, Michiels C, Alexandre I, Remacle J. Effect of hypoxia upon intracellular calcium concentration of human endothelial cells. *J Cell Physiol*. 1992;152:215–21.
23. Suresh K, Servinsky L, Jiang H, Bigham Z, Yun X, Kliment C, et al. Reactive oxygen species induced Ca(2+) influx via TRPV4 and microvascular endothelial dysfunction in the SU5416/hypoxia model of pulmonary arterial hypertension. *Am J Physiol Lung Cell Mol Physiol*. 2018;314:893–907.
24. Mungai PT, Waypa GB, Jairaman A, Prakriya M, Dokic D, Ball MK, et al. Hypoxia triggers AMPK activation through reactive oxygen species-mediated activation of calcium release-activated calcium channels. *Mol Cell Biol*. 2011;31:3531–45.
25. Gusarova GA, Trejo HE, Dada LA, Briva A, Welch LC, Hamanaka RB, et al. Hypoxia leads to Na, K-ATPase downregulation via Ca(2+) release-activated Ca(2+) channels and AMPK activation. *Mol Cell Biol*. 2011;31:3546–56.
26. Zeng B, Liao X, Liu L, Ruan H, Zhang C. Thyroid hormone diminishes Ca2+ overload induced by hypoxia/reoxygenation in cardiomyocytes by inhibiting late sodium current and reverse-Na+/Ca2+ exchange current. *Pharmacology*. 2020;105:63–72.
27. Hamdollah Zadeh MA, Glass CA, Magnussen A, Hancox JC, Bates DO. VEGF-mediated elevated intracellular calcium and angiogenesis in human microvascular endothelial cells in vitro are inhibited by dominant negative TRPC6. *Microcirculation*. 2008;15:605–14.
28. Desireddi JR, Farrow KN, Marks JD, Waypa GB, Schumacker PT. Hypoxia increases ROS signaling and cytosolic Ca(2+) in pulmonary artery smooth muscle cells of mouse lungs slices. *Antioxid Redox Sign*. 2010;12:595–602.
29. Monsel A, Zhu YG, Gennai S, Hao Q, Liu J, Lee JW. Cell-based therapy for acute organ injury: preclinical evidence and ongoing clinical trials using mesenchymal stem cells. *Anesthesiology*. 2014;121:1099–121.
30. Berridge MJ, Bootman MD, Roderick HL. Calcium signalling: dynamics, homeostasis and remodelling. *Nat Rev Mol Cell Biol*. 2003;4:517–29.
31. Bootman MD, Berridge MJ, Roderick HL. Calcium signalling: more messengers, more channels, more complexity. *Curr Biol*. 2002;12:R563–5.
32. Aley PK, Porter KE, Boyle JP, Kemp PJ, Peers C. Hypoxic modulation of Ca2+ signaling in human venous endothelial cells. Multiple roles for reactive oxygen species. *J Biol Chem*. 2005;280:13349–54.
33. Baudin B, Bruneel A, Bosselut N, Vaubourdolle M. A protocol for isolation and culture of human umbilical vein endothelial cells. *Nat Protoc*. 2007;2:481–5.
34. Pati S, Khakoo AY, Zhao J, Jimenez F, Gerber MH, Harting M, et al. Human mesenchymal stem cells inhibit vascular permeability by modulating vascular endothelial cadherin/beta-catenin signaling. *Stem Cells Dev*. 2011;20:89–101.
35. Gnecci M, Melo LG. Bone marrow-derived mesenchymal stem cells: isolation, expansion, characterization, viral transduction, and production of conditioned medium. *Methods Mol Biol*. 2009;482:281–94.
36. Ribeiro V, Garcia M, Oliveira R, Gomes PS, Colaco B, Fernandes MH. Bisphosphonates induce the osteogenic gene expression in co-cultured human endothelial and mesenchymal stem cells. *J Cell Mol Med*. 2014;18:27–37.
37. Unger RE, Sartoris A, Peters K, Motta A, Migliaresi C, Kunkel M, et al. Tissue-like self-assembly in cocultures of endothelial cells and osteoblasts and the formation of microcapillary-like structures on three-dimensional porous biomaterials. *Biomaterials*. 2007;28:3965–76.
38. Laranjeira MS, Fernandes MH, Monteiro FJ. Reciprocal induction of human dermal microvascular endothelial cells and human mesenchymal stem cells: time-dependent profile in a co-culture system. *Cell Prolif*. 2012;45:320–34.
39. Lennikov A, Mirabelli P, Mukwaya A, Schaupper M, Thangavelu M, Lachota M, et al. Selective IKK2 inhibitor IMD0354 disrupts NF-kappaB signaling to suppress corneal inflammation and angiogenesis. *Angiogenesis*. 2018;21:267–85.
40. Palmer AE, Jin C, Reed JC, Tsien RY. Bcl-2-mediated alterations in endoplasmic reticulum Ca2+ analyzed with an improved genetically encoded fluorescent sensor. *Proc Natl Acad Sci U S A*. 2004;101:17404–9.
41. Zhang X, Rodriguez-Nino A, Pastene DO, Pallavi P, van den Born J, Bakker SJL, et al. Methylglyoxal induces p53 activation and inhibits mTORC1 in human umbilical vein endothelial cells. *Sci Rep*. 2021;11:8004.
42. Maier P, Herskind C, Fleckenstein K, Spier I, Laufs S, Zeller WJ, et al. MDR1 gene transfer using a lentiviral SIN vector confers radioprotection to human CD34+ hematopoietic progenitor cells. *Radiat Res*. 2008;169:301–10.
43. Park JG, Palmer AE. Verifying the function and localization of genetically encoded Ca2+ sensors and converting FRET ratios to Ca2+ concentrations. *Cold Spring Harb Protoc*. 2015;2015:pdb.prot076547.
44. Meyer AJ, Dick TP. Fluorescent protein-based redox probes. *Antioxid Redox Sign*. 2010;13:621–50.
45. Yan K, Zheng J, Zollner FG, Schwenke K, Pallavi P, Keese M. A modified surgical model of hind limb ischemia in ApoE<sup>-/-</sup> mice using a miniature incision. *J Vis Exp*. 2021;171:e62402.
46. Tarlov IM. Spinal cord compression studies. III. Time limits for recovery after gradual compression in dogs. *AMA Arch Neurol Psychiatry*. 1954;71:588–97.

47. Westvik TS, Fitzgerald TN, Muto A, Maloney SP, Pimiento JM, Fancher TT, et al. Limb ischemia after iliac ligation in aged mice stimulates angiogenesis without arteriogenesis. *J Vasc Surg*. 2009;49:464–73.
48. Gijbels MJ, van der Cammen M, van der Laan LJ, Havekes LM, Hofker MH, et al. Progression and regression of atherosclerosis in APOE3-Leiden transgenic mice: an immunohistochemical study. *Atherosclerosis*. 1999;143:15–25.
49. Sharov VS, Dremina ES, Galeva NA, Williams TD, Schoneich C. Quantitative mapping of oxidation-sensitive cysteine residues in SERCA in vivo and in vitro by HPLC-electrospray-tandem MS: selective protein oxidation during biological aging. *Biochem J*. 2006;394:605–15.
50. Cook NL, Viola HM, Sharov VS, Hool LC, Schoneich C, Davies MJ. Myeloperoxidase-derived oxidants inhibit sarco/endoplasmic reticulum Ca<sup>2+</sup>-ATPase activity and perturb Ca<sup>2+</sup> homeostasis in human coronary artery endothelial cells. *Free Radic Biol Med*. 2012;52:951–61.
51. Ronkainen VP, Skoumal R, Tavi P. Hypoxia and HIF-1 suppress SERCA2a expression in embryonic cardiac myocytes through two interdependent hypoxia response elements. *J Mol Cell Cardiol*. 2011;50:1008–16.
52. Pietrobon D, Di Virgilio F, Pozzan T. Structural and functional aspects of calcium homeostasis in eukaryotic cells. *Eur J Biochem*. 1990;193:599–622.
53. Malhotra JD, Kaufman RJ. The endoplasmic reticulum and the unfolded protein response. *Semin Cell Dev Biol*. 2007;18:716–31.
54. Lamalice L, Le Boeuf F, Huot J. Endothelial cell migration during angiogenesis. *Circ Res*. 2007;100:782–94.
55. Gover-Proaktor A, Granot G, Shapira S, Raz O, Pasvolksy O, Nagler A, et al. Ponatinib reduces viability, migration, and functionality of human endothelial cells. *Leuk Lymphoma*. 2017;58:1455–67.
56. Almeria C, Weiss R, Roy M, Tripisciano C, Kasper C, Weber V, et al. Hypoxia conditioned mesenchymal stem cell-derived extracellular vesicles induce increased vascular tube formation in vitro. *Front Bioeng Biotechnol*. 2019;7:292.
57. Gong LC, Xu HM, Guo GL, Zhang T, Shi JW, Chang C. Long non-coding RNA H19 protects H9c2 cells against hypoxia-induced injury by targeting microRNA-139. *Cell Physiol Biochem*. 2017;44:857–69.
58. Cha HH, Hwang JR, Sung JH, Choi SJ, Oh SY, Roh CR. Changes in calcium channel proteins according to magnesium sulfate administration in placentas from pregnancies with pre-eclampsia or fetal growth restriction. *J Investig Med*. 2019;67:319–26.
59. Thompson MD, Mei Y, Weisbrod RM, Silver M, Shukla PC, Bolotina VM, et al. Glutathione adducts on sarcoplasmic/endoplasmic reticulum Ca<sup>2+</sup>-ATPase Cys-674 regulate endothelial cell calcium stores and angiogenic function as well as promote ischemic blood flow recovery. *J Biol Chem*. 2014;289:19907–16.
60. Evangelista AM, Thompson MD, Weisbrod RM, Pimental DR, Tong X, Bolotina VM, et al. Redox regulation of SERCA2 is required for vascular endothelial growth factor-induced signaling and endothelial cell migration. *Antioxid Redox Sign*. 2012;17:1099–108.
61. Cerra MC, Imbrogno S. Phospholamban and cardiac function: a comparative perspective in vertebrates. *Acta Physiol (Oxf)*. 2012;205:9–25.
62. Shintani-Ishida K, Yoshida K. Ischemia induces phospholamban dephosphorylation via activation of calcineurin, PKC- $\alpha$ , and protein phosphatase 1, thereby inducing calcium overload in reperfusion. *Biochim Biophys Acta*. 2011;1812:743–51.
63. Marks AR. Calcium cycling proteins and heart failure: mechanisms and therapeutics. *J Clin Invest*. 2013;123:46–52.
64. Rodriguez P, Kranias EG. Phospholamban: a key determinant of cardiac function and dysfunction. *Arch Mal Coeur Vaiss*. 2005;98:1239–43.
65. Panieri E, Santoro MM. ROS signaling and redox biology in endothelial cells. *Cell Mol Life Sci*. 2015;72:3281–303.
66. Stavely R, Nurgali K. The emerging antioxidant paradigm of mesenchymal stem cell therapy. *Stem Cells Transl Med*. 2020;9:985–1006.
67. Chen MF, Lin CT, Chen WC, Yang CT, Chen CC, Liao SK, et al. The sensitivity of human mesenchymal stem cells to ionizing radiation. *Int J Radiat Oncol Biol Phys*. 2006;66:244–53.
68. Qin HH, Filippi C, Sun S, Lehec S, Dhawan A, Hughes RD. Hypoxic preconditioning potentiates the trophic effects of mesenchymal stem cells on co-cultured human primary hepatocytes. *Stem Cell Res Ther*. 2015;6:237.
69. Lan YW, Choo KB, Chen CM, Hung TH, Chen YB, Hsieh CH, et al. Hypoxia-preconditioned mesenchymal stem cells attenuate bleomycin-induced pulmonary fibrosis. *Stem Cell Res Ther*. 2015;6:97.
70. Ezquer M, Urzua CA, Montecino S, Leal K, Conget P, Ezquer F. Intravitreal administration of multipotent mesenchymal stromal cells triggers a cytoprotective microenvironment in the retina of diabetic mice. *Stem Cell Res Ther*. 2016;7:42.
71. Ma Z, Song G, Zhao D, Liu D, Liu X, Dai Y, et al. Bone marrow-derived mesenchymal stromal cells ameliorate severe acute pancreatitis in rats via hemeoxygenase-1-mediated anti-oxidant and anti-inflammatory effects. *Cytotherapy*. 2019;21:162–74.
72. Vilaca-Faria H, Salgado AJ, Teixeira FG. Mesenchymal stem cells-derived exosomes: a new possible therapeutic strategy for Parkinson's disease? *Cells*. 2019;8:118.
73. Liu K, Ji K, Guo L, Wu W, Lu H, Shan P, et al. Mesenchymal stem cells rescue injured endothelial cells in an in vitro ischemia-reperfusion model via tunneling nanotube like structure-mediated mitochondrial transfer. *Microvasc Res*. 2014;92:10–8.
74. Hellingman AA, Bastiaansen AJ, de Vries MR, Seghers L, Lijkwan MA, Lowik CW, et al. Variations in surgical procedures for hind limb ischaemia mouse models result in differences in collateral formation. *Eur J Vasc Endovasc Surg*. 2010;40:796–803.
75. Bers DM. Cardiac sarcoplasmic reticulum calcium leak: basis and roles in cardiac dysfunction. *Annu Rev Physiol*. 2014;76:107–27.

## Publisher's Note

Springer Nature remains neutral with regard to jurisdictional claims in published maps and institutional affiliations.

Ready to submit your research? Choose BMC and benefit from:

- fast, convenient online submission
- thorough peer review by experienced researchers in your field
- rapid publication on acceptance
- support for research data, including large and complex data types
- gold Open Access which fosters wider collaboration and increased citations
- maximum visibility for your research: over 100M website views per year

At BMC, research is always in progress.

Learn more [biomedcentral.com/submissions](https://biomedcentral.com/submissions)

